Implementing deep soil and dynamic root uptake in Noah-MP (v4.5): Impact on Amazon dry-season transpiration

Carolina A. Bieri[1], Francina Dominguez[1], Gonzalo Miguez-Macho[2], and Ying Fan[3]

[1]Department of Climate, Meteorology, and Atmospheric Sciences, University of Illinois Urbana-Champaign, Urbana, Illinois, USA

[2]Nonlinear Physics Group, Faculty of Physics, Universidade de Santiago de Compostela, Santiago de Compostela, Galicia, Spain

[3]Department of Earth and Planetary Sciences, Rutgers University, New Brunswick, New Jersey, USA

Correspondence: Francina Dominguez (francina@illinois.edu)

Abstract. Plant roots act as critical pathways of moisture from the subsurface to the atmosphere. Deep moisture uptake by plant roots can provide a seasonal buffer mechanism in regions with a well-defined dry season such as the southern Amazon. Here, mature forests maintain transpiration (a critical source of atmospheric moisture in this part of the world) during drier months. Most existing state-of-the-art earth system models do not have the necessary features to simulate subsurface-to-atmosphere moisture variations during drydowns. These features include groundwater dynamics, a sufficiently deep soil column, dynamic root water uptake (RWU), and a fine model spatial resolution (<5 km).

To address this, we present DynaRoot, a dynamic root water uptake scheme implemented in the Noah-Multi-Parameterization (Noah-MP) land surface model, a widely used model for studying kilometer-scale regional land surface processes. Our modifications include the implementation of DynaRoot, eight additional resolved soil layers reaching a depth of 20 m, and soil properties that vary with depth. DynaRoot is computationally efficient and ideal for regional- or continental-scale climate simulations. We perform four 20-year uncoupled Noah-MP experiments for a region in the southern Amazon basin. Each experiment incrementally adds physical complexity. The experiments include default Noah-MP with free drainage (FD); a case with an activated groundwater scheme that resolves water table variations (GW); a case with eight added soil layers and soil properties that vary with depth (SOIL); and a case with DynaRoot activated (ROOT).

Our results show that DynaRoot allows mature forests in upland regions to avoid water stress during dry periods by taking up moisture from the deep vadose zone (where antecedent precipitation is still draining downward). Conversely, RWU in valleys can access moisture from groundwater (while remaining constrained by the water table). Temporally, we capture a seasonal shift in RWU from shallower layers in wetter months to deeper soil layers in drier months, particularly over regions with dominant evergreen broadleaf (forest) vegetation. Compared to the control case, there is a domain-average increase in transpiration of about 29% during dry months in the ROOT experiment. Critically, the ROOT experiment performs best in simulating the temporal evolution of dry-season transpiration, using an observations-based ET product as reference. Future work will explore the effect of the DynaRoot uptake scheme on atmospheric variables in a coupled modeling framework.

1 Introduction

The Amazon region of South America is a critical terrestrial source of atmospheric moisture. Evapotranspiration (ET) from the Amazon basin, defined as the combination of transpiration and evaporation from canopy and ground surfaces, has been estimated to be about 1100 mm year^{-1} (Baker et al., 2021). Wei et al. (2017) found the ratio of transpiration to ET (excluding evaporation from canopy interception) to be highest in the Amazon out of any other region in the world, around 85%. ET is particularly important for Amazonian hydroclimate, as the proportion of precipitation that originates from local ET—known as the recycling ratio—is estimated to be between 25 and 40% (Dominguez et al., 2022). During drier months (approximately June through September), the southern Amazon is a net source of moisture, as evaporation exceeds precipitation (Zemp et al., 2014). Given the importance of Amazon ET for the water budget of the region, accurate representation of processes which influence ET in numerical models is critical. More generally, the earth system modeling community has expressed the need for improved representation of soil hydrology, groundwater variations, and representation of root water uptake (RWU) in global models (Kleidon and Heimann, 2000; Feddes et al., 2001; Pitman, 2003; Fan et al., 2017; Kendon et al., 2021).

During dry months, Amazonian canopies maintain greenness (Saleska et al., 2007) and avoid water stress, resulting in maintenance of dry season ET (Nepstad et al., 1994; Kim et al., 2012; Morton et al., 2014). Previous studies suggest this is due to several possible mechanisms: nighttime transfer of water from dry to moist areas by roots (known as hydraulic redistribution; Oliveira et al., 2005b), deep RWU (Nepstad et al., 1994), and groundwater capillary rise (Markewitz et al., 2010). The importance of a particular mechanism could depend on location (Christoffersen et al., 2014) or multiple mechanisms could operate in synergy (Baker et al., 2009). In this work, we focus on deep RWU given the plentiful evidence for its importance in areas with seasonal dryness (Nepstad et al., 1994; Jipp et al., 1998; von Randow et al., 2004; Davidson et al., 2011; Ivanov et al., 2012; Broedel et al., 2017; Fan et al., 2017; Smith and Boers, 2023).

Deep moisture uptake by roots can be thought of as a 'buffer' during seasonally dry periods, allowing vegetation to access deep vadose zone moisture when surface moisture from precipitation is not sufficient (Nepstad et al., 1994; Jipp et al., 1998; Baker et al., 2009). Smith and Boers (2023) posited that deep-rooted vegetation is more resilient during dry periods. Miguez-Macho and Fan (2021) found that 18% of global annual transpiration originates as deeper soil and rock moisture; in August, this percentage was estimated to be 60-90% in the southern Amazon. Soil moisture observations collected by Bruno et al. (2006) in an Amazonian forest reflected withdrawal of soil moisture up to 10 m below the surface. Broedel et al. (2017) collected soil moisture observations from the central Amazon and found root uptake below 4.8 m during a year that was exceptionally dry. In a modeling study of an artificial throughfall exclusion experiment at Tapajós National Forest in northern Brazil (Nepstad, 2002; Nepstad et al., 2007; Davidson et al., 2011), Markewitz et al. (2010) noted that while the percentage of RWU occurring at depths between 5.5 and 11.5 m was relatively small (10%), model results suggest it was critical to survival. Thus, while the actual amount of deep RWU may be small compared to uptake from shallower depths, it can have an outsized effect on the the vitality of vegetation.

As outlined in Fan et al. (2017) and Miguez-Macho and Fan (2021), topography influences both root access to deep moisture and the source of this moisture. In very low areas with waterlogging, roots do not grow deep to avoid oxygen stress. A synthesis

of more than 2,000 root observations by Fan et al. (2017) supports this. Moisture flowing downgradient from higher elevations supports valley vegetation via remote recharge; critically, this source accounts for up to 47% of dry-month RWU (Miguez-Macho and Fan, 2021). In upland regions where the water table is very deep, roots become decoupled from it, but rely on moisture from previous precipitation (which infiltrates slowly downwards) in the deep vadose zone. It is in midslope and upland areas that we expect roots to tap into deep moisture during dry months. The influence of drainage gradient on RWU source is further explored in Miguez-Macho and Fan (2021).

Most state-of-the-art earth system models do not currently include an integrated representation of groundwater, deep resolved soil layers and dynamic RWU. Table 1 summarizes existing representation of fine-scale groundwater variations and deep, dynamic RWU in regional land models. Moreover, we consider whether these models can be coupled to a convection-permitting atmospheric model (CPM), since adequate representation of convective precipitation is highly relevant to the hydrological cycle in many parts of the world, including the Amazon (Rehbein et al., 2018). All of the models in Table 1 – with the exception of Noah-MP and ISAM – were employed in the Coupled Model Intercomparison Project Phase 6 (CMIP6; Eyring et al. 2016). To our knowledge, six of the nine models listed in Table 1 include some representation of deep or dynamic RWU in their official releases, but most do not include both. Only three models (CLM, JSBACH and GFDL LM) include sufficiently deep resolved soil layers to model deep roots in the Amazon. We consider hydrologically active layers extending to 5 m or below to be sufficient based on observations (Restom and Nepstad, 2004; Bruno et al., 2006; Davidson et al., 2011; Fan et al., 2017; Broedel et al., 2017). We consider dynamic RWU to be uptake that varies with time and/or moisture content. Four of the nine models include a groundwater scheme that simulates a lower boundary below the soil column in the form of an aquifer (as opposed to free-draining conditions). One model includes all of the features considered in Table 1, the Community Land Model (CLM) of the Community Earth System Model (CESM; Lawrence et al. 2019). We note that representation of deep, dynamic RWU has been included in model versions that have not been distributed publicly and/or included in an official release. We do not consider such contributions in Table 1, and instead provide a summary of these efforts in Table 2.

Water table depth variations are best simulated using a fine spatial scale ($<$5 km) to adequately resolve small-scale topographical features that determine local drainage networks (Fan et al., 2013; Barlage et al., 2021). Advances in groundwater parameterizations – such as the scheme designed and validated in Fan et al. (2007) and Miguez-Macho et al. (2007) – have made it possible to model these fine-scale features. Inclusion of the Miguez-Macho et al. (2007) groundwater scheme (designated as the Miguez-Macho and Fan, or MMF scheme, for the remainder of this publication) in a model used to simulate regional climate has made it possible to discern links between subsurface moisture variations and land surface fluxes that influence atmospheric heat and moisture budgets, as well as precipitation (Martinez et al., 2016a, b; Barlage et al., 2021).

From Table 1, we see that most existing regional climate models do not offer sufficient capability to fully resolve the soil-root-atmosphere moisture pathway, neglecting a vital source of moisture for phreatophytic vegetation and potentially introducing biases in soil moisture, land-atmosphere fluxes and near-surface atmospheric variables. From Table 2, we see that representations of deep, dynamic RWU that do exist involve more complexity than needed for our purposes or do not include both deep and dynamic RWU. To address the need for more representative deep vadose zone hydrology, including RWU, we introduce a modified version of Noah-MP that incorporates three major enhancements: 1) DynaRoot, a RWU scheme described

in Fan et al. (2017) that can be seamlessly coupled to deep vadose zone moisture variations and is computationally efficient; 2) an increase in the number of resolved soil layers from four to twelve with an according increase in cumulative depth from 2 m to 20 m; 3) an updated definition of soil properties, which vary with depth based on exponential decay functions without additional input data from the user. Modifications 2 and 3 are necessary for the implementation of DynaRoot.

We implement DynaRoot in the Noah-MultiParameterization model, or Noah-MP (Niu et al., 2011). We select Noah-MP for this work since it is commonly used as a land surface parameterization for the Weather Researching and Forecasting (WRF) model (Skamarock et al., 2021), a widely used numerical weather model ideal for resolving fine spatial scales. Although we focus on uncoupled Noah-MP simulations in this study, in the future we will evaluate the impact of deep RWU on atmospheric variables in a coupled land-atmosphere framework. The WRF model is ideal for simulating the atmosphere on spatial scales that can resolve atmospheric convection. Moreover, we can capture fine-scale variations in water table depth on these smaller scales, allowing us to simulate the important connection between RWU and groundwater variations. The fact that the MMF scheme is already implemented in Noah-MP further supports our decision to implement DynaRoot in this model (Barlage et al., 2015; Martinez et al., 2016a, b). Finally, we focus our efforts on Noah-MP because it is one of the three models listed in Table 1 that currently includes no representation of deep or dynamic RWU in its official release. Yet, the Noah-MP/WRF framework is frequently employed in studies of regional climate (Barlage et al., 2015; Martinez et al., 2016a, b; Spera et al., 2018; Fersch et al., 2020; Schwitalla et al., 2020; Barlage et al., 2021; Dominguez et al., 2024).

To focus our work and demonstrate the functionality of our Noah-MP modifications, we test four hypotheses:

- H1: Access to moisture from groundwater is critical for valley vegetation.
- H2: Deep vadose zone moisture is critical for upland vegetation.
- H3: Dynamic root uptake, according to the soil water profile, is most important during dry months and sustains transpiration.
- H4: Dynamic root uptake is more prevalent and more strongly influences transpiration for mature forests, which exhibit deeper uptake profiles compared to non-forested areas.

This research is an important step towards more physically realistic simulation of the biophysical link between the subsurface and atmospheric branches of the hydrologic cycle in the model. Critically, this framework can be used on spatial scales that are most relevant for land-atmosphere fluxes. These developments can be valuable contributions to the larger Noah-MP and land surface modeling community, and will allow others to more effectively explore science questions regarding the role of vegetation in regional hydroclimate.

2 Methods

2.1 Description of default Noah-MP

In this study, we use the High-Resolution Land Data Assimilation System (HRLDAS) Noah-MP version 4.5 (https://github.com/NCAR/hrldas/tree/release-v4.5-WRF; Chen et al. 2007), which is consistent with version 4.5 of WRF (https://github.com/wrf-model/WRF/tree/release-v4.5; Skamarock et al. 2021). We use the model in its default state as the control configuration in the suite of simulations described in section 2.3 of the Methods.

A common method of Noah-MP initialization is to provide a file generated by the WRF Pre-Processing System (WPS; https://github.com/wrf-model/WPS). Model input files from WRF WPS provide initial values for variables such as soil moisture, soil temperature, and equilibrium water table depth, and also define static variables such as vegetation type and dominant soil texture for the domain. There are several vegetation datasets available in WPS; we use the default 21-class Moderate Resolution Imaging Spectroradiometer (MODIS) land use dataset in all simulations. Outside of the United States, dominant soil texture data in WPS is sourced from the Food and Agriculture Organization (FAO) Soil Map of the World (FAO/UNESCO, 1971).

Default Noah-MP includes four resolved soil layers which extend to 2 m depth. There are several options for determining soil properties in the model. In our control configuration, we employ the default option in which soil properties are determined by the dominant soil texture at a given grid cell and do not vary with depth. Soil moisture at saturation, saturated hydraulic conductivity, saturated hydraulic diffusivity, soil moisture at wilting point, and saturated soil matric potential, among other soil properties, are defined in a lookup table. In default Noah-MP, root depth for a given grid point is also specified via a lookup table and is based on the dominant vegetation type at that point. The root depth determines the soil layers from which moisture for transpiration is extracted via RWU. It does not change with time or moisture content.

In Noah-MP, RWU for a given soil layer j is calculated as

$$RWU_j = s_j T \tag{1}$$

where T is transpiration at a given grid cell, and

$$s_j = \beta_j = \begin{cases} \frac{\theta_j - \theta_{wilt_j}}{\theta_{ref_j} - \theta_{wilt_j}} & Noah \\ \frac{\psi_{wilt_j} - \psi_j}{\psi_{wilt_j} + \psi_{sat_j}} & CLM \\ 1 - e^{-5.8 \ln \frac{\psi_{wilt_j}}{\psi_j}} & SSiB \end{cases} \tag{2}$$

depending on the option for calculation of β_j (known as the soil moisture stress factor) set by the user (Niu et al., 2011). Several options are available, including Noah type, CLM type, and SSiB type formulations. θ_j (ψ_j) is soil moisture (soil matric potential) for layer j, θ_{wilt_j} (ψ_{wilt_j}) is the wilting point soil moisture (wilting point soil matric potential), ψ_{sat_j} is saturated soil matric potential, and θ_{ref_j} is the reference soil moisture. See Niu et al. (2011) for further details on the formulation of β_j in Noah-MP.

2.2 Description of modified Noah-MP

2.2.1 Additional soil layers

Soil layer depths as defined in our modified Noah-MP simulations are shown in Table 3. We add eight soil layers, bringing the total number to 12 with a cumulative depth of 20 m. This means hydrologically active soil layers in modified Noah-MP are deep enough to capture RWU consistent with uptake depths in the Amazon observed or inferred to be 4.8-18 m (Davidson et al., 2011; Bruno et al., 2006; Broedel et al., 2017). This is not the case in default Noah-MP. As WRF WPS only provides initial values for the original four soil layers in default Noah-MP, it is necessary to obtain initial values of soil moisture and temperature for the additional resolved layers in our modified setup. We assigned soil moisture to these layers via a calculated equilibrium profile based on initial water table values from WRF WPS. The details of this process are included in the appendix.

2.2.2 Varying soil properties with depth

It is critical to capture observed decreases in porosity and permeability of geologic materials with depth (Fan et al., 2007), particularly in the case of a deeper resolved soil column in our modified Noah-MP setup. Parameterization options that allow varying soil properties with depth are included in Noah-MP, but their use requires additional soil input data for the added layers. These data are not possible to obtain at the depths and spatial resolution we are concerned with. Thus, we implement exponential decay functions that can describe changes in soil properties with depth on kilometer scales (Miguez-Macho and Fan, 2012):

$$\psi_{sat_j} = \psi_{sat_\circ} \exp \frac{z_j - 1.5}{f} \tag{3}$$

$$\theta_{sat_j} = \theta_{sat_\circ} \exp \frac{-z_j + 1.5}{f} \tag{4}$$

$$\theta_{wilt_j} = \theta_{wilt_\circ} \exp \frac{-z_j + 1.5}{f} \tag{5}$$

$$K_{sat_j} = K_{sat_\circ} \exp \frac{-z_j + 1.5}{f} \tag{6}$$

$$D_{sat_j} = \frac{-K_{sat_j} \psi_{sat_j} b}{\theta_{sat_j}} \tag{7}$$

where K_{sat_j} is saturated soil hydraulic conductivity, D_{sat_j} is saturated soil diffusivity, f is the e-folding depth for permeability, b is the Clapp–Hornberger exponent corresponding to the grid point dominant soil type (Clapp and Hornberger, 1978), and z_j is the midpoint of soil layer j. The midpoint of each soil layer is expressed relative to 1.5 m depth, ensuring that soil properties do not vary in the top 4 shallow soil layers. Variables with a nought subscript indicate the value of that variable in the first soil layer. Details of the calculation of f are found in Fan et al. (2007) and Miguez-Macho and Fan (2012). f is higher in flat sedimentary basins and lower for steep mountain slopes, which reflects the fact that steep slopes shed sediments while valleys accumulate them. Equation (7) was derived based on Darcy's law describing flow through a porous medium.

As part of the MMF groundwater scheme, a variably thick soil layer is added at grid points where the water table is below the resolved soil layers (Miguez-Macho et al., 2007). This layer extends from the bottom of the lowest resolved layer to the

water table. Soil properties for the variably thick layer are also based on the exponential decay functions shown above, with z set to a constant (22.5 m) for simplicity regardless of the thickness of the layer.

2.2.3 The DynaRoot scheme

Following Fan et al. (2017), DynaRoot is analogous to Ohm's law of current flow between two points given a potential difference and conductor resistance. RWU happens preferentially in layers with lower resistance (wetter and shallower layers). Vegetation relies on RWU from higher-resistance layers (drier and deeper layers) only when the soil water profile "allows" it. In other words, DynaRoot simulates plant behavior of balancing need for water with the effort required for uptake.

The scheme is composed of two main functions. These include an ease function (e_j) calculated at each soil layer (j) and a fractional contribution to RWU for each soil layer (r_j), known as the root activity function:

$$e_j = \frac{\psi_j - \psi_{lmin}}{\frac{2}{3}h_{veg} + z_j} \tag{8}$$

$$r_j = \frac{e_j \Delta z_j}{\sum_{j=1}^{n} e_j \Delta z_j} \tag{9}$$

where ψ_{lmin} is the minimum leaf water potential (set as a constant to -204 m, or -2 MPa), h_{veg} is the vegetation canopy height corresponding to the grid point dominant vegetation type, n is the number of resolved soil layers, and Δz_j is the thickness of soil layer j. The ease function e_j is based on the concept that RWU is influenced by the local soil water profile, which is determined by both infiltration from above and interactions with groundwater from below. For further information on the conceptual basis of DynaRoot, see the supplementary information provided in Fan et al. (2017). DynaRoot is added as a new module in the energy subroutine in modified Noah-MP. The values of e_j and r_j are calculated in the new module. In the water subroutine of Noah-MP, r_j replaces the beta factor β_j for soil moisture stress such that $s_j = r_j$ in Eq. (2).

Moreover, soil layers can be designated as having active or inactive root activity. This is determined by the value of e_j. If the value of e_j for layer j is zero for one model year, that layer is flagged as inactive. The layer can only become active again if it is the easiest layer from which to take up moisture; i.e., if the value of e_j exceeds the value of e_j everywhere else in the soil column. Additionally, in modified Noah-MP root depth at a given grid point is allowed to vary in time. Soil layers with active RWU comprise the root zone; the root depth is designated as the depth of the deepest layer with active root uptake.

In modified Noah-MP, we calculate the maximum depth of RWU, D_{RWU}, as the soil layer j at which $\sum_{j=1}^{n} r_j T >= 0.95T$. If T is zero, D_{RWU} is set to the depth of the first resolved layer (0.1 m). DynaRoot constrains RWU to soil layers above the water table. If the water table is calculated to be above the bottom of the first resolved soil layer, RWU is constrained to that layer.

We do not employ Noah-MP's crop model in any of our simulations to lessen complexity and avoid additional computational cost. Given this, we do not expect our results to be reliable in areas with crop irrigation.

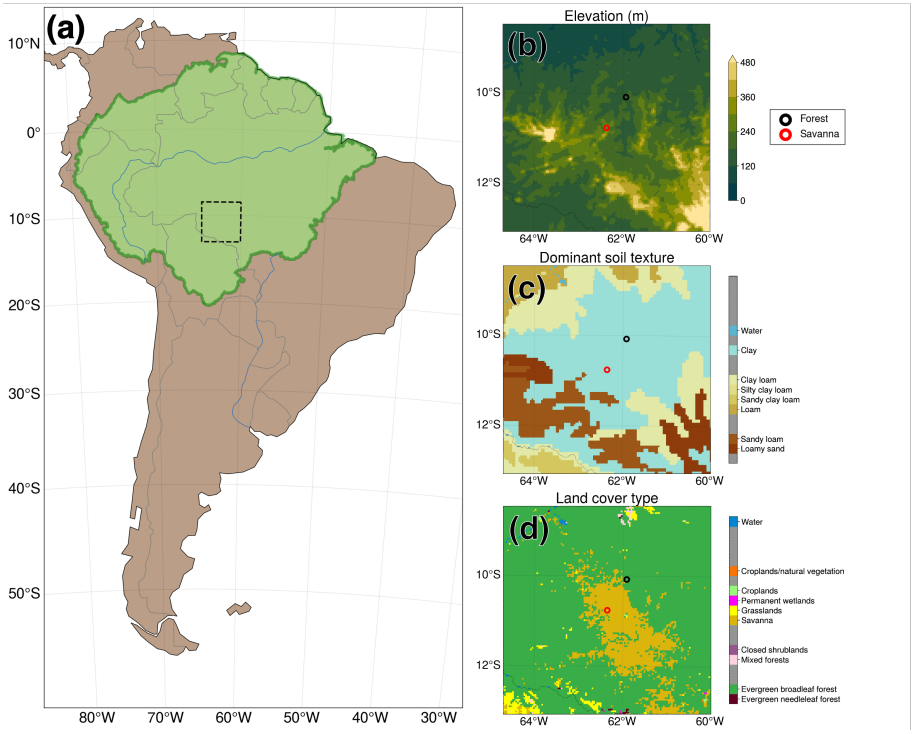

Figure 1. Location of Noah-MP simulation domain and static input fields derived from WRF WPS. (a) Location of Noah-MP simulation domain for all cases (black dashed box). The green shaded area denotes the boundaries of the Amazon basin. Made with Natural Earth (public domain). (b) Elevation in the simulation domain. (c) Grid point dominant soil texture. (d) Similar to (c), but for grid point dominant vegetation.

2.3 Description of Noah-MP simulations

We ran modified Noah-MP for a domain located in the southern Amazon, within the Brazilian state of Rondônia. Figure 1 depicts the simulation domain within South America (1a), elevation (1b), dominant soil texture (1c), and vegetation cover (1d) as defined in our simulations. We selected a relatively small region that would allow us to carry out a proof of concept for our modified version of Noah-MP. We sought a domain which includes areas designated as needing deep soil water, as has been done in studies such as Nepstad et al. (1994).

Table 4 lists the Noah-MP cases analyzed in this study: FD (free drainage), GW (MMF groundwater scheme activated), SOIL (identical to GW but with additional soil layers), and ROOT (identical to SOIL but with DynaRoot activated). FD acts as the control case in this study. The experimental design allows us to test the hypotheses listed in the Introduction. GW corresponds to H1, enabling us to test the effect of groundwater convergence in valleys on uptake. The SOIL experiment aids in testing H2, with deeper resolved soil layers that can store past precipitation in the deep vadose zone. Finally, the ROOT experiment simulates vegetation reliance on deep RWU via the DynaRoot uptake scheme, allowing us to test H3 and H4. The incremental

nature of the cases (increasing in complexity from FD to ROOT) allows us to isolate the effect of individual physics and modifications.

All simulations were offline, i.e. the model was run in an uncoupled state without active interaction between land and atmospheric components. Rather, 3 hourly atmospheric forcing data with the exception of precipitation were sourced from the Global Land Data Assimilation System (GLDAS; Rodell et al. 2004; Beaudoing et al. 2020). Precipitation data were sourced from the Integrated Multi-satellitE Retrievals for GPM (IMERG) product (Huffman et al., 2023). Simulations were completed for a nearly 20-year period from 01 Jun 2000 to 31 December 2019. In all simulations, the model was run at a 4 km resolution and 30 min time step. Model output for the first three years was discarded in our analysis to account for model spin up; about three years of model integration are required for soil moisture in the deepest layers to stabilize. Also, the DynaRoot uptake scheme is not fully active until one year into the model integration. Additional simulation setup details are shown in Table 5. GLDAS data were processed and converted to the necessary format using scripts provided with the HRLDAS source code. IMERG precipitation rate data were processed separately; data were averaged into 3 hourly intervals and regridded to the resolution of the Noah-MP simulations. All simulations were performed on the National Center for Atmospheric Research (NCAR) Derecho supercomputer (Computational and Information Systems Laboratory, 2024).

2.4 Comparison with observations-based data

We compared Noah-MP transpiration to gridded data from the Global Land Evaporation Amsterdam Model v3.8a (GLEAM; Miralles et al., 2011; Martens et al., 2017). GLEAM provides estimates of ET and its components via a set of algorithms applied to satellite observations (Martens et al., 2017). An important limitation of GLEAM is the soil module used in deriving the evaporation estimates, which includes shallow soil layers that only extend to 2.5 m (Martens et al., 2017). Despite this limitation, GLEAM is valuable in its temporal availability and partitioning of ET into components. We note that flux tower data is available within our domain from the Large-Scale Biosphere-Atmosphere Experiment in Amazonia (LBA; Restrepo-Coupe et al., 2021). However, these data are only available for the early 2000s, coinciding with years that were discarded from the model output to account for spin up of deep soil layers.

We apply the Mann–Kendall test for monotonic trend (Mann, 1945; Kendall, 1948; Gilbert, 1987) to the mean time series of transpiration and ET between days 150 and 250 of the year (the height of the dry season) for each point in the domain. We then calculate the slope of the Mann–Kendall trend (known as the Theil-Sen estimator) for the mean time series for each point (Theil, 1950; Sen, 1968). The sign of the Theil-Sen estimator indicates the direction of the trend in the mean time series; a positive (negative) value is associated with generally increasing (decreasing) transpiration or ET. We compare spatial patterns of the Theil–Sen estimator between the SOIL and ROOT Noah-MP model runs and the gridded GLEAM evaporation estimates.

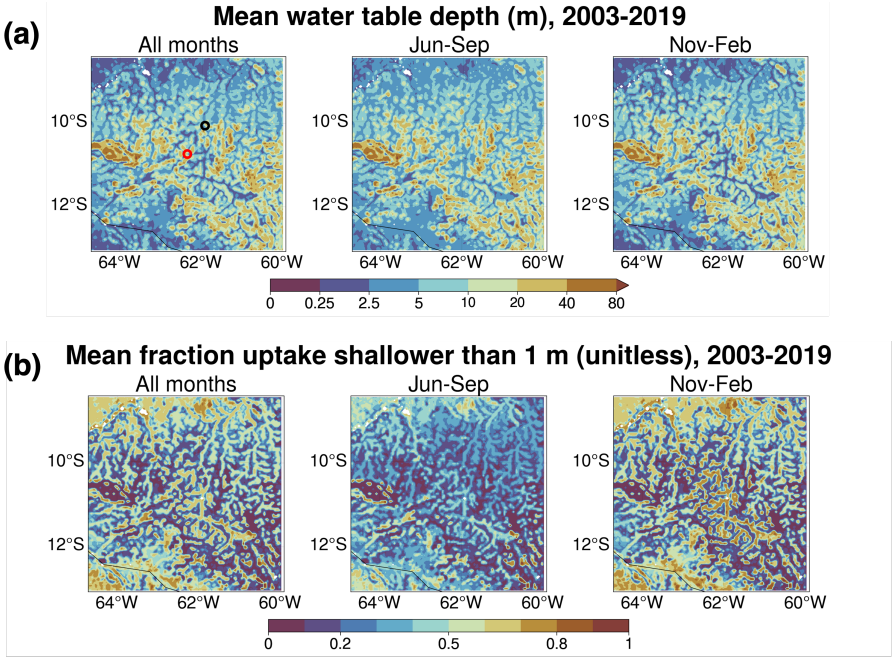

Figure 2. Simulation mean results from the ROOT experiment. (a) Simulation mean WTD for all months (left), relatively dry months (Jun-Sep; center), and wet months (Nov-Feb; right). (b) Simulation mean fraction of uptake shallower than 1 m for all months (left), relatively dry months (Jun-Sep; center), and wet months (Nov-Feb; right).

3 Results

3.1 Noah-MP model output

Figure 2 depicts simulation mean water table depth (WTD) and uptake shallower than 1 m in the ROOT experiment for all months, relatively dry months (Jun-Sep), and wet months (Nov-Feb). Mean WTD is generally deeper in drier months (Fig. 2a), reflecting seasonal availability of moisture from precipitation. WTD is consistent with simulated values for the same region from other studies (Martinez et al., 2016a; Fan et al., 2017). Fractional uptake shallower than 1 m (Fig. 2b) varies between dry and wet periods, with a clear shift in uptake to depths below 1 m during drier months. This is consistent with a seasonal shift in RWU from shallower to deeper areas of the root zone as moisture from precipitation becomes scarce during drier months.

We examine model output at the point scale to gain an understanding of localized interplay between groundwater, soil moisture, RWU, and land surface fluxes with and without our Noah-MP modifications. We analyze output for two points in the domain, a point with dominant evergreen broadleaf forest and a point with dominant savanna vegetation. The locations of these points are shown in Fig. 1. Given the mean water table locations at these points, we expect uptake to tap into groundwater capillary rise at the savanna point (in line with H1) and deep vadose zone uptake to occur at the forest point (in line with H2). We expect dry-season deep RWU to be more relevant at the forest point compared to the savanna point, in accordance with

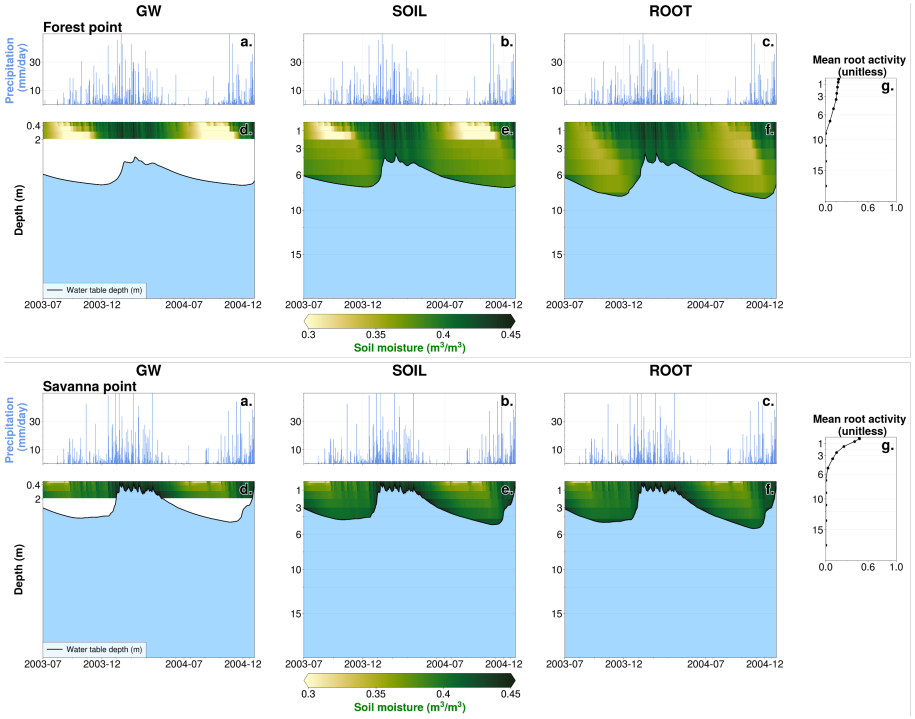

Figure 3. Noah-MP model output, 07-2003 to 12-2004. (a)-(c), top row: Mean daily precipitation rate for GW, SOIL, and ROOT experiments at the forest point. (d)-(f), top row: Mean daily soil moisture (shading) and WTD (black line) for GW, SOIL, and ROOT experiments at the forest point. Light blue shading represents regions below the water table. (g), top row: Simulation mean root activity r_j at the forest point (from the ROOT case). (a)-(g), bottom row: Identical to (a)-(g) in the top row but for the savanna point.

H3 and H4. Note that deep-rooted woody vegetation has been shown to exist in savanna ecosystems (Canadell et al., 1996; Oliveira et al., 2005a; Singh et al., 2020). Most of the areas classified as savanna in our domain are a result of deforestation, with forest giving way to grass-dominant pastures with a shallower rooting depth (Gash and Nobre, 1997; Roberts et al., 2002; Von Randow et al., 2004; Piontekowski et al., 2019; Honey, 2023). Additionally, Noah-MP does not capture heterogeneity in growth form within a given vegetation class, making it impossible for us to account for the proportion of potentially deep-rooted woody vegetation in savanna. A single canopy height range is assumed for every grid point classified as savanna (minimum 0.1 m, maximum 10 m) and forest (minimum 8 m, maximum 20 m). This canopy height is considered in calculation of e_j.

The point-level time series of 1.5 years of model output (Figure 3) support all four hypotheses. In the GW case, locally higher values of soil moisture exist in the vicinity of the water table at the savanna point (Fig 3d, bottom), consistent with capillary rise. The rooting depth at this point (static at 1 m in this experiment) would allow vegetation to tap into this moisture source, consistent with H1. However, there is a disconnect between resolved soil layers (which extend to a cumulative depth of 2 m) and the water table for both forest and savanna points (Figs. 3d, top and 3d, bottom) during all or part of the period. Direct interaction between resolved soil layers and the water table can only occur when the water table is 2 m or shallower.

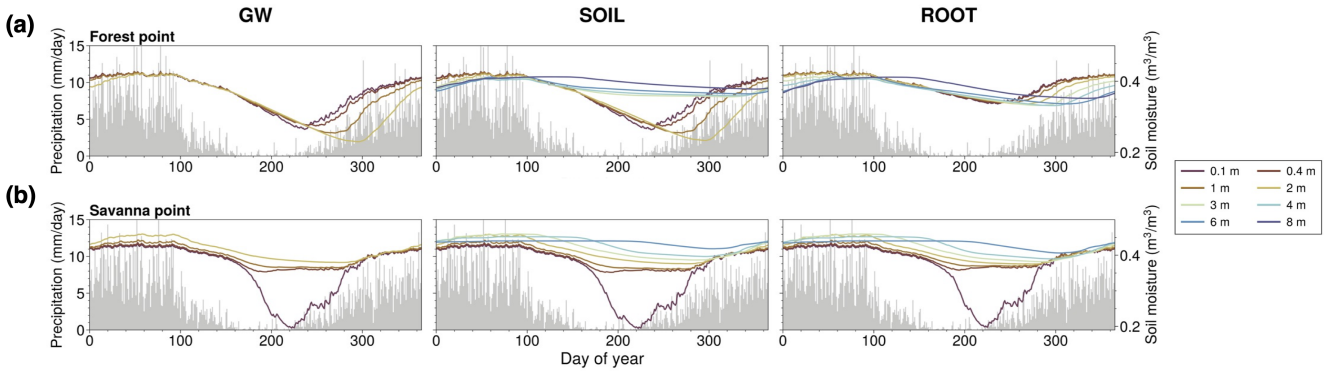

Figure 4. (a) Day of year mean soil moisture (multicolored lines) and precipitation (grey bars) for GW, SOIL, and ROOT cases at the forest point. (b) Identical to (a), but for the savanna point. Note that soil moisture is only plotted for layers above the water table.

When the water table is deeper than 2 m, indirect interaction occurs via the artificial variably thick layer that extends from the bottom of resolved soil layers to the water table.

In the SOIL experiment, the additional soil layers enable direct interaction between resolved layers and the water table at both points. Periodic decreases in shallow soil moisture occur at the forest point in SOIL (light yellow colors in Figs. 3d and 3e, top). These periods of decreased soil moisture roughly align with seasonally dry periods (Figs. 3a and 3b, top). There is a noticeable discontinuity in soil moisture at 2 m depth at the forest point. This is due to the prescribed rooting depth, which is fixed and constrained to 2 m in the SOIL experiment. With the added soil layers in this case, Fig 3e (top) reflects the added soil moisture store in the deep vadose zone, which cannot be fully accessed unless RWU is allowed to extend deeper (H2). At the savanna point, the seasonal depletion of shallow moisture is not as present, signifying a lack of dependence on root uptake (H4). The vadose zone is not as deep, supporting the accessibility of moisture for uptake in the capillary fringe (H1).

In the ROOT experiment – identical to the SOIL setup but with the DynaRoot uptake scheme activated – seasonal soil moisture changes are more uniformly distributed throughout the soil layers, resulting in less shallow soil drying during drier months. This is especially clear at the forest point (Fig. 3f, top). Figure 3g (top) confirms deep and more uniform RWU with depth at the forest point, as non-zero mean root activity r_j values extend up to the eighth soil layer (which has a layer bottom that corresponds to 8 m). These results are in support of H2 and H3. When deep moisture is available, vegetation will access it, particularly in drier months when surface moisture from precipitation is not sufficient. The source of this moisture is the deep vadose zone, where moisture from past precipitation is stored. Conversely, Fig. 3g (bottom) confirms less reliance on deep RWU at the savanna point in the ROOT case, as r_j drops off exponentially from its maximum in the shallowest soil layer. At the same time, r_j at this point indicates that uptake occurs such that vegetation can tap into groundwater capillary rise, supporting H1. The mean root activity profiles and soil moisture variations at each point illustrate the dependence of DynaRoot on vegetation type, in support of H4.

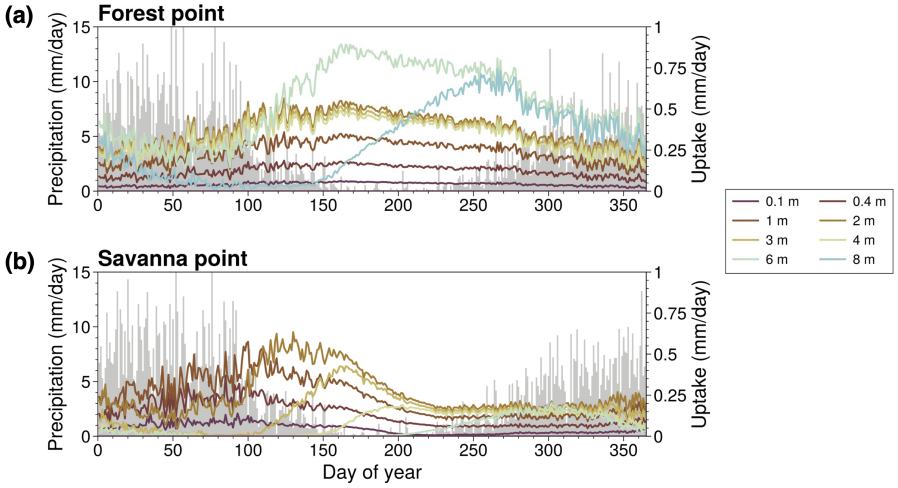

Figure 5. (a) Day of year mean RWU (multicolored lines) and precipitation (grey bars) for the ROOT experiment at the forest point. (b) Identical to (a), but for the savanna point.

Figure 4 shows the mean seasonal cycle of soil moisture for multiple soil layers at the forest point (Fig. 4a) and the savanna point (Fig. 4b) and for GW (left), SOIL (center), and ROOT (right). We also show precipitation for reference. In the GW case at the forest point (Fig. 4a), soil moisture in all layers is nearly identical until approximately mid-August, when soil moisture in shallower layers begins to rebound from an annual minimum value. Soil moisture in deeper layers continues to decrease before rebounding by late October. At the savanna point (Fig. 4b), soil moisture in deeper layers varies little throughout the year compared to the shallowest layer, which exhibits mostly constant behavior followed by a precipitous decline at the end of the dry season and a sharp rebound. In the SOIL experiment, additional deep soil layers do not affect the behavior of soil moisture in shallower layers, which exhibit nearly identical behavior to GW at both points. This is due to the fact that rooting depth is consistent with unmodified Noah-MP in this experiment, constrained to a 2 m maximum depth. In the ROOT case, soil moisture in shallow layers shows less of a decline throughout the year at the forest point, while deeper layers show a gradual depletion throughout the dry season compared to SOIL. As such, with the addition of deep soil layers and dynamic RWU, water uptake is more uniformly distributed throughout the soil column during the dry season and transition to the wet season. At the savanna point, results are relatively unchanged in ROOT, SOIL, and GW. These findings support H3 (dynamic RWU is critical in the dry season) and H4 (dynamic RWU is more important for mature forests compared to non-forested areas).

The behavior suggested by Fig. 4 is further supported by Fig. 5, showing the mean seasonal cycle of RWU in the ROOT case at the forest point (Fig. 5a) and the savanna point (Fig. 5b). For reference, the annual precipitation cycle is depicted in these plots as well. At the forest point, RWU predominantly occurs in deeper layers in the dry season. During other times of the year, the magnitude of deep RWU is more comparable to RWU in shallower layers. The clear seasonal behavior of RWU exhibited at the forest point is consistent with seasonal dependence on deep RWU in forested areas of the Amazon (Nepstad

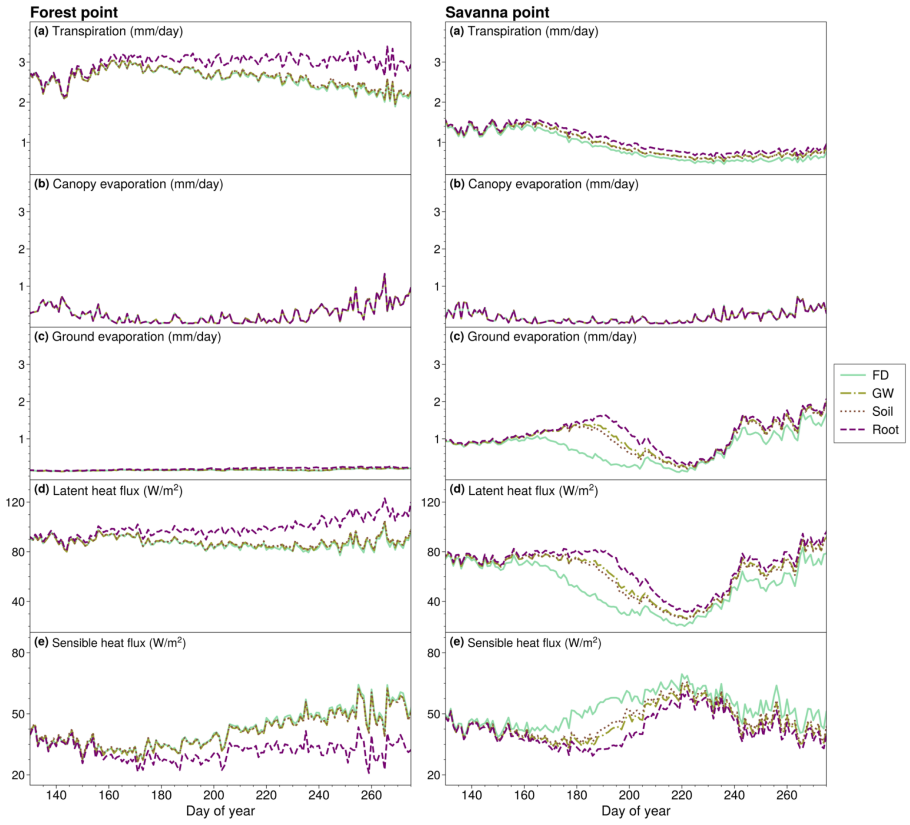

Figure 6. (a)-(e), left: Day of year mean (a) transpiration, (b) canopy evaporation, (c) ground evaporation, (d) latent heat flux, and (e) sensible heat flux for FD, GW, SOIL, and ROOT cases at the forest point. (a)-(e), right: Identical to left panel, but for the savanna point.

et al., 1994; Markewitz et al., 2010; Ivanov et al., 2012), consistent with H3 and H4. Notably, RWU in the deepest layer shown in Fig. 5a is near zero in the first part of the year and quickly ramps up as the dry season progresses. At the savanna point, RWU predominantly occurs in shallower layers. Seasonal changes in RWU are also evident at the savanna point; RWU peaks around the end of the wet season and quickly declines through the dry season. This behavior indicates the lack of reliance on RWU at the savanna point compared to forest; RWU is not maintained through the dry season as it is at the forest point. These findings are supportive of H3 and H4.

Annual mean land surface fluxes at the forest and savanna points, including transpiration, latent heat flux, sensible heat flux, ground evaporation, and canopy evaporation, are depicted in Fig. 6. Results for all four cases – FD, GW, SOIL, and ROOT – are plotted. We show results for the dry season and transition to the wet season (days 130 to 270 of the year) as fluxes do not differ between cases during other parts of the year. In the ROOT experiment at the forest point (Fig. 6, left column), we see an increase (decrease) in transpiration and latent heat flux (sensible heat flux) compared to other simulations from approximately day 160 (early June) through day 270 (mid-October). Importantly, changes in fluxes are only associated with

the ROOT experiment which includes DynaRoot. Transpiration increases in accordance with increased availability of moisture at depth in the ROOT experiment at the forest point (Figs. 3f, top and 4a). This result is in accordance with H3. As there is nearly zero change in canopy or ground evaporation (Figs. 6b and 6c, left), changes in latent heat flux (6d, left) can be attributed to changes in transpiration that result from addition of DynaRoot. This is what we expect given that greater plant access to deep moisture should be reflected in transpiration as opposed to surface or canopy evaporation. Importantly, we note that in the ROOT case, the magnitude of change in surface fluxes increases throughout the dry season and into the transition to the wet season at the forest point.

In contrast to the forest point, the annual mean cycle of dry-season transpiration at the savanna point (Fig. 6a, right column) shows little change throughout the year in all cases compared to FD. Increases in latent heat flux (Fig. 6d) and decreases in sensible heat flux (Fig. 6e) are highest in the early dry season and predominantly occur in the GW and ROOT cases. Given that there is little change in transpiration at the savanna point, changes in latent heat flux must be attributable to other components of surface evaporation. This is shown by the mean annual cycle of dry-season ground evaporation at the savanna point (Fig. 6c, right), which increases early on and evolves similarly to latent heat flux. We speculate that the increase in early dry-season ground evaporation is tied to increases in soil moisture associated with an active GW scheme in the GW and SOIL cases and more uniform (yet shallow) RWU with depth in the ROOT case. Given the shallow root activity profile at the savanna point (Fig. 3g, bottom) and lack of change in dry-season transpiration (Fig. 6a, right), we deduce that changes in the surface energy balance are not associated with enhanced uptake as a result of adding DynaRoot. These results support H4.

We present a regional analysis to highlight geographical variations within the domain. Figure 7 depicts the seasonal mean difference in transpiration between FD and all other simulations averaged over all years of model output. As expected from the point analysis, differences are minimal during wetter seasons (DJF and MAM) and largely positive during drier seasons (JJA and SON). In SON, when the greatest difference between runs is calculated, the domain average percent difference between the ROOT and FD experiments is about 29%, corresponding to an increase in domain mean transpiration of 0.46 mm day^{-1}. Regarding the spatial distribution of transpiration differences in Fig. 7, there is a visible pattern consistent with mean WTD simulated by the model (Fig. 2). Critically, transpiration differences between GW and FD (Fig. 7a) in JJA and SON are mostly in lower-lying areas, where we expect moisture from groundwater to influence soil moisture and in turn, transpiration (Miguez-Macho and Fan, 2021). This result supports H1. Transpiration differences between ROOT and FD (Fig. 7c) in JJA and SON are non-negligible in areas with a higher drainage position, suggesting that upland vegetation tap into moisture in the deep vadose zone when DynaRoot is activated. This finding is consistent with H2 and H3. Moreover, differences in transpiration reflect the dominant vegetation cover at each grid point (Fig. 1); differences are generally larger for forested grid points in agreement with the point analysis and H4.

We calculated probability density functions (PDFs) of mean dry-season transpiration for the simulation with only deep soils (SOIL) and the simulation with deep soils and DynaRoot (ROOT). We analyze points with a mean water table that is 2.5 m or shallower in the dry season, points with a dry-season mean water table between 2.5 m and 20 m, and points with a dry-season mean water table below 20 m. These PDFs are shown in Fig. 8. We expect to see the DynaRoot uptake scheme mainly impacting midslope (Fig. 8b) and upland points (Fig. 8c) where uptake from the deep vadose zone is important (in accordance

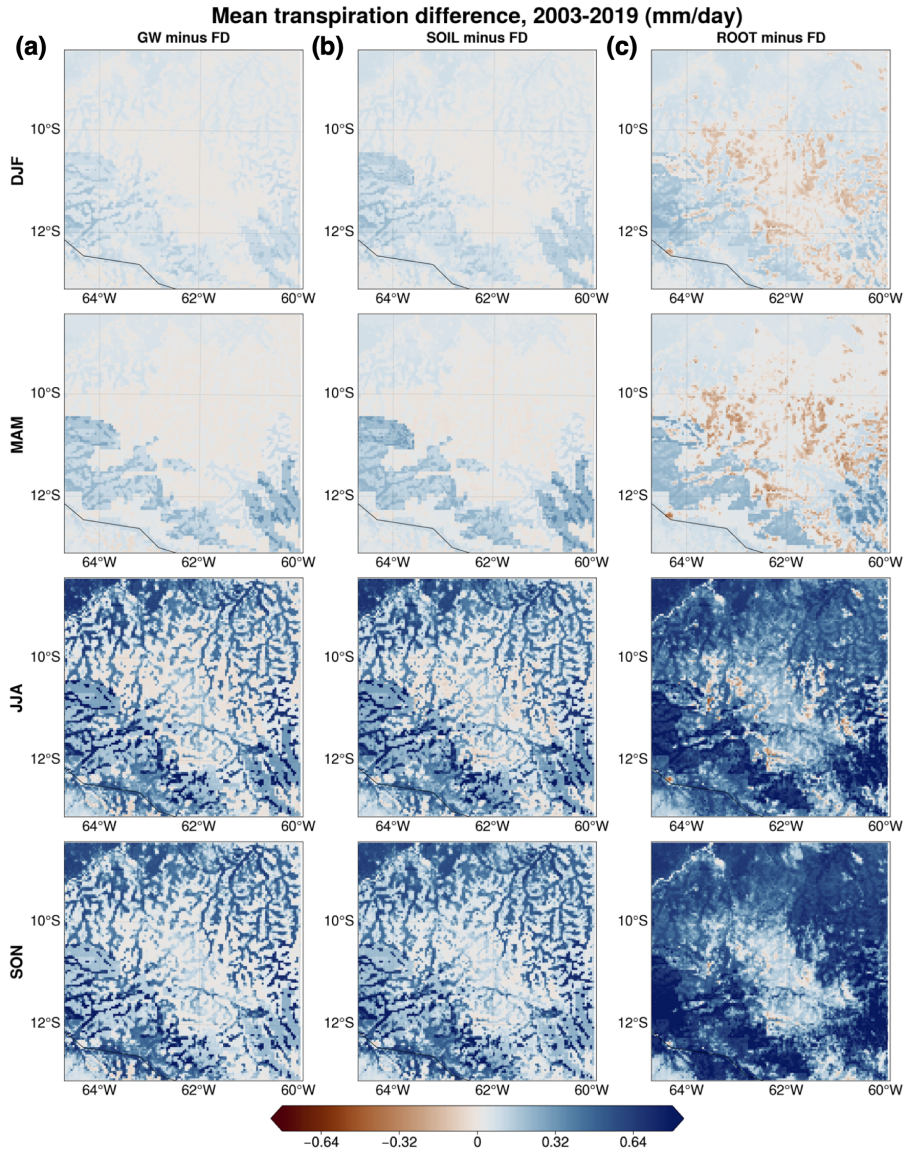

Figure 7. Seasonal mean transpiration differences between (a) GW and FD, (b) SOIL and FD, and (c) ROOT and FD.

with H2). This is indeed what we see in Figs. 8a-8c, with the activation of DynaRoot resulting in a more noticeable shift towards higher values of dry-season transpiration in Figs. 8b and 8c compared to Fig. 8a. This is particularly true for Fig. 8b, which corresponds to points with mean dry-season WTD between 2.5 m and 20 m.

Additionally, we calculated PDFs of mean dry-season transpiration for points with evergreen broadleaf dominant vegetation (forested) and savanna dominant vegetation (non-forested; Figs. 8d and 8e). We see a greater impact at forested points where LAI is higher and we expect vegetation to be more dependent on deep RWU during the dry season. While there seems to be

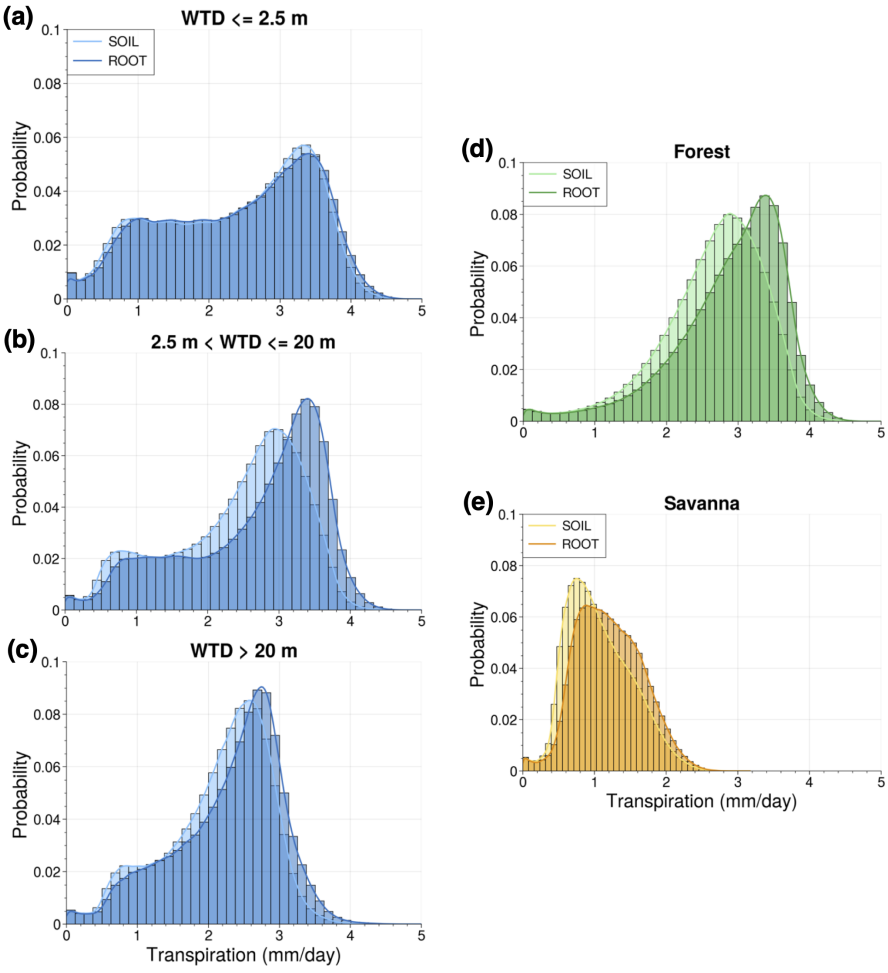

Figure 8. Probability density functions depicting distribution of SOIL and ROOT mean dry-season transpiration for different groupings of grid points: (a) Points with mean shallow WTD (<= 2.5 m) in the dry season, (b) points with mean dry-season WTD between 2.5 m and 20 m, (c) points with mean dry-season WTD below 20 m, (d) points with evergreen broadleaf forest dominant vegetation, and (e) points with savanna dominant vegetation.

somewhat of a shift towards higher values of dry-season transpiration for savanna points (Fig. 8e), there is a much clearer shift for forested points (Fig. 8d). This result is supportive of H4.

3.2 Comparison with observations-based ET product

One of the difficulties in evaluating our model results via comparison to observations is the very limited number of eddy covariance observations in the region, and large uncertainties in ET estimates using remote sensing (Baker et al., 2021). As

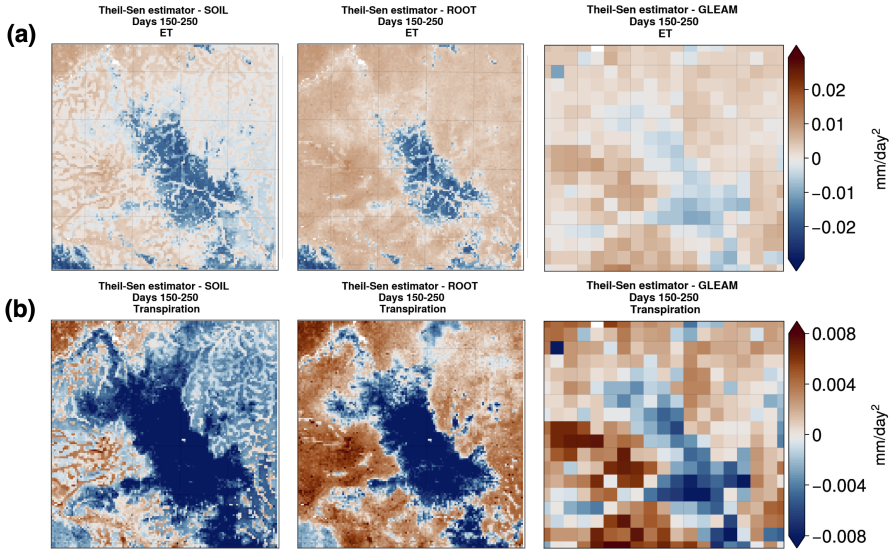

Figure 9. (a) Theil-Sen slope for mean ET and (b) transpiration between days 150 and 250 of the year for the SOIL (left column) and ROOT (middle column) Noah-MP experiments and GLEAM (right column) transpiration and ET.

an alternative to validation via direct comparison, we can evaluate how the addition of DynaRoot affects dry-season dynamics when compared to observations-based estimates. Dry season behavior reflects the resilience of forest vs. savanna vegetation during periods of water stress, and can have an important effect on sub-seasonal surface flux interactions with the overlying atmosphere.

To assess the ability of modified Noah-MP to represent dry-season transpiration and ET dynamics, we perform a comparison with GLEAM data. In Fig. 9a, we see that the Theil–Sen slope (Theil, 1950; Sen, 1968) for ET is generally negative for non-forested areas with savanna and positive for forested areas with evergreen broadleaf vegetation in Noah-MP. This is especially true in the ROOT experiment. We see that with the addition of DynaRoot the sign of the Theil–Sen slope for ET exhibits slightly more agreement with GLEAM than results from the SOIL experiment. To further quantify this, we remapped the Noah-MP and GLEAM ET and transpiration fields to the GLEAM resolution ($0.25°$), determined the Theil-Sen slopes, and calculated the Pearson correlation coefficient between the SOIL case, ROOT case, and GLEAM. The Pearson correlation with GLEAM increases only slightly between the SOIL and ROOT cases, from 0.586 to 0.588.

Focusing on transpiration in Fig. 9b, we see that, generally speaking, negative Theil–Sen slopes are calculated for model grid points with savanna and positive slopes are calculated for forested points. Exceptions to this are present in the eastern part of the domain in the SOIL experiment. This is where vegetation is largely classified as evergreen broadleaf forest, but the Theil–Sen slope is generally negative. Comparing with slopes calculated from GLEAM transpiration estimates, we see that results from the ROOT experiment are more in line with observations-based estimates. The Pearson correlation between the

SOIL (ROOT) slopes and GLEAM slopes is 0.592 (0.649), further supporting this. Keeping in mind the shallow soil module used to produce the GLEAM estimates, we note that GLEAM values may be lower than if deeper soils were included.

Overall, we can glean something critical from Fig. 9: Addition of the DynaRoot uptake scheme results in dry-season evolution of transpiration that is more in line with observations-based estimates than a Noah-MP configuration without it. This highlights the role of DynaRoot in realistically simulating dry-season surface flux dynamics at the land-atmosphere interface. Moreover, this result is in support of H3, as we show that inclusion of deep, dynamic RWU is necessary to realistically model the mean evolution of dry-season transpiration for this domain.

4 Discussion

Overall, we find that the results of this work support the hypotheses detailed in the Introduction and are in accordance with previous studies that motivated these hypotheses. These include Fan et al. (2017), which highlighted the importance of groundwater as a moisture source for vegetation during dry periods, and Miguez-Macho and Fan (2021), which clarified that while moisture from groundwater is important in valleys, deep vadose zone storage of past precipitation is critically important in uplands during dry months. Additionally, the findings of this study are in line with others listed in Table 2, all of which found that inclusion of deep and/or dynamic RWU in Noah-MP improved model performance (Gayler et al., 2014; Wang et al., 2018; Liu et al., 2020; Niu et al., 2020; Li et al., 2021). In particular, Niu et al. (2020) and Li et al. (2021) noted improvements in Noah-MP's performance during drier periods after enhancements were made. Zanin (2021) is the only study in Table 2 that focused on the Amazon region and included the domain for this study. They compared their model results to flux tower data from the LBA project. Similar to our work, they found changes in seasonality of soil moisture in shallow and deep layers resulting from addition of deep RWU. While simulation of sensible heat flux improved in Zanin (2021) when deep RWU was activated, latent heat flux was overestimated. However, seasonality of evapotranspiration was reduced.

The results of this work reflect an advancement in the representation of the link between subsurface and atmospheric fluxes of moisture via RWU in the offline configuration of Noah-MP. To demonstrate this, we focus on a region centered on the state of Rôndonia in the southern Amazon. The structure of the model in its default state made it impossible to represent time-varying moisture uptake from subsurface sources below 2 m depth, a critical source of dry-season moisture in southern Amazon forests. Now, we have a way of representing seasonal reliance of vegetation on deep RWU. Moreover, with the availability of an active groundwater scheme in Noah-MP, we can study the interplay between groundwater, soil moisture, roots, and land surface fluxes. This allows us to more fully resolve moisture pathways from the subsurface to the atmosphere, enabling future studies that continue to investigate the role of deep RWU in modulating vegetation water stress and determining atmospheric moisture availability. This is especially important as the Amazon is projected to experience drier conditions in the future as a result of climate change (Joetzjer et al., 2013) and the ecosystem's drought resilience may be at risk (Chen et al., 2024).

Additionally, in this work we have described an approach to account for variations in soil properties with depth. Such properties are constant through the soil profile in unmodified Noah-MP unless the user provides input soil texture data for each layer. We incorporate exponential decay functions that describe changes in soil properties with depth without the need for

additional user-provided data. This enhances the realism of the model with minimal overhead and facilitates simulations with additional deep soil layers.

We focus on the Amazon region in this work because of its critical importance for global climate (Werth and Avissar, 2002; Liu et al., 2023). However, our modified model would be useful in simulating any ecosystem where vegetation has adapted to periodic water stress. The simplicity of DynaRoot is ideal for coupling with atmospheric models with high computational overhead such as WRF, providing a realistic approach to accounting for critical land surface and subsurface processes in a coupled land–atmosphere modeling framework without added parameters or calibration.

We note that the DynaRoot uptake scheme does not consider the role of carbon availability in determining RWU depth and the presence of roots; rather, it depends solely on the soil water profile. While the role of carbon is certainly relevant to studies focused on directly simulating root growth based on principles of plant physiology and resource acquisition, here we focus on hydrologically based rooting depth, allowing the soil water profile to drive root growth. This is sufficient for the scope of our work, without the use of an active dynamic vegetation module that would predict resource-based rooting growth. We elect to run simulations without such a module in the interest of minimizing complexity and computational cost.

5 Conclusions

5.1 Summary of findings

This work details implementation of a deep, dynamic RWU scheme known as DynaRoot in the Noah-MP land surface model. The conceptual details of this scheme are outlined in Fan et al. (2017). DynaRoot makes it possible to capture deep, dynamic RWU based on the local soil water profile, which was not previously possible in Noah-MP. Additionally, DynaRoot allows us to obtain a measure of rooting depth based on the depth of RWU. In addition to implementing DynaRoot, we enhanced other parts of Noah-MP, including addition of eight resolved soil layers and varying soil properties with depth.

Previous studies have illustrated the crucial reliance of Amazonian forests on deep RWU via observational (Nepstad et al., 1994; Bruno et al., 2006; Broedel et al., 2017) and modeling-based (Kleidon and Heimann, 2000; Markewitz et al., 2010) methods, supporting our focus on this region in this work. We completed several offline Noah-MP simulations for a domain in the southern Amazon. These cases include an out-of-the-box unmodified Noah-MP case with free drainage (FD), which acts as a control configuration, an unmodified Noah-MP case with a groundwater scheme activated (GW), a modified Noah-MP case with additional resolved soil layers and soil properties that vary with depth (SOIL), and a modified Noah-MP case identical to SOIL but with the DynaRoot uptake scheme activated (ROOT). Each case facilitates testing of a different hypothesis. Our main findings are listed below:

- At the savanna point, capillary rise in the vicinity of the water table is simulated. Mean root activity indicates uptake sourced from the capillary fringe, consistent with H1. RWU predominantly occurs in shallower layers and maximizes early in the dry season.

- At the forest point, RWU shifts to the deep vadose zone during the dry season, supporting H2, H3, and H4. The seasonal cycle of RWU indicates deeper RWU at the forest point during the dry season compared to the savanna point, further supporting H4.

- Dry-season transpiration and latent heat flux (sensible heat flux) increase (decreases) as a result of adding DynaRoot, signifying a change in surface energy flux partitioning. Changes in latent heat flux at the forest point are mostly accounted for by changes in transpiration, while changes in latent heat flux at the savanna point are accounted for by changes in ground evaporation likely unrelated to deep RWU. Changes in surface fluxes are in accordance with H3 and H4.

- Domain-averaged increase in transpiration between the ROOT and FD experiments is about 29%, corresponding to an increase in transpiration of 0.46 mm day^{-1}.

Comparison of our simulation results with GLEAM remote sensing-based estimates of dry-season moisture fluxes for the domain reveal that dry-season temporal evolution of transpiration in forested areas better agrees with GLEAM in the ROOT case (DynaRoot activated) compared to the SOIL case (DynaRoot not activated). These results confirm the value of our Noah-MP modifications in realistically capturing seasonal moisture flux dynamics at the land-atmosphere interface in an ecosystem that is dependent on deep RWU to buffer rainfall deficits. Moreover, the results of this comparison provide further support for H3.

5.2 Significance and future work

Critically, the changes to Noah-MP outlined in this work mean we now have a numerical model that can capture the spectrum of interactions from groundwater through deep soil and plant roots to the atmosphere via transpiration. To our knowledge, no existing land-atmosphere modeling framework includes sufficient representation of all these components to capture the influence of groundwater and the local soil moisture profile on rooting depth for convection-resolving simulations. We plan to implement our enhancements in the community version of Noah-MP to facilitate access to the DynaRoot scheme within the larger land-atmosphere modeling community. In the meantime, access to the version of the model used for this study is provided in an online repository (see the code and data availability section below).

Noah-MP with DynaRoot enabled can be used to investigate a number of different science questions with wide-ranging implications. Given the role of plant trait diversity in resilience of the Amazon as studied by Sakschewski et al. (2016) and the identification of deep-rooting as a drought resilience strategy by Chen et al. (2024), DynaRoot could be used to study changes in forest resilience under deforestation scenarios. Moreover, given that moisture varies slowly in subsurface soils (Amenu et al., 2005), DynaRoot makes it possible to characterize the role of deep soil moisture memory in influencing surface moisture via transpiration in a coupled land-atmosphere framework. Such research has been alluded to in Niu et al. (2020) and Zanin (2021), and could have implications for predictability of atmospheric moisture on longer timescales. Dominguez et al. (2024) discuss two multidecadal convection-permitting simulations that were completed for the entire South American continent. In their analysis of these runs, Zilli et al. (2024) identified land-atmosphere coupling in CPMs as an outstanding area of investigation. This motivates potential future work that focuses on the role of fine-scale land surface characteristics—such as water table

depth and vegetation traits (including rooting depth)—in simulating convection. DynaRoot would be applicable in such work, particularly in global convection-permitting simulations that have become a priority in the climate modeling community (Satoh et al., 2019; Caldwell et al., 2021; Feng et al., 2023).

Future work will focus on further validating these efforts by comparing modeled root depth with remote sensing-based root depth estimates, which offer more spatiotemporal coverage than in-situ data. An additional goal in the future is to complete coupled Noah-MP and WRF simulations that will allow us to investigate some of the science questions mentioned in the previous paragraph. As we strive to understand the state of our changing world, it is more imperative than ever to adequately characterize vegetation and its influence on hydroclimate in critical ecosystems such as the Amazon.

Code and data availability. The version of HRLDAS Noah-MP used in this study is available at https://doi.org/10.5281/zenodo.13137185. Model configuration, input, and forcing files are available at https://doi.org/10.5281/zenodo.13061970. Scripts used to process, analyze, and plot model and observations-based data are available at https://doi.org/10.5281/zenodo.13137808.

Atmospheric forcing data used for the model simulations in this study are publicly available online. GLDAS data are available from https://ldas.gsfc.nasa.gov/gldas. IMERG data are available from https://gpm.nasa.gov/data/imerg. Static input data used for the model simulations are available at https://www2.mmm.ucar.edu/wrf/users/download/get_sources_wps_geog.html. The base HRLDAS Noah-MP source code and documentation are available at https://github.com/NCAR/hrldas. WRF WPS source code and documentation are available at https://github.com/wrf-model/WPS. GLEAM ET and transpiration data used in this study are available at https://www.gleam.eu. The Amazon basin shapefile used to generate Fig. 1 is available at https://github.com/gamamo/AmazonBasinLimits.

Appendix A: Initialization procedure for additional soil layers

Initial soil moisture values for layers 5 through twelve were derived using a formulation of the Richards equation describing water flow in unsaturated soils:

$$q_j = \frac{1}{2} D_{sat_j} \frac{(\theta_j - \theta_{j+1})}{\Delta z_j} + K_{sat_j} (\frac{\theta_j}{\theta_{sat_j}})^{b+1} \tag{A1}$$

where q_j is the flux of water between a soil layer j and the layer below it $j+1$, D_{sat_j} is saturated soil hydraulic diffusivity, θ_j is soil moisture in soil layer j, Δz_j is the thickness of soil layer j, K_{sat_j} is saturated hydraulic conductivity, θ_{sat_j} is soil moisture at saturation, and b is the Clapp–Hornberger exponent corresponding to the grid point dominant soil type (Clapp and Hornberger, 1978). We assume q_j to be zero at the initial time step for simplicity.

Equilibrium WTD, which is sourced from the input file generated by WRF WPS, is used for the initial WTD values. The details of how the equilibrium WTD data were created can be found in Fan et al. (2007). Given the equilibrium WTD at a given grid point, we can infer θ_j at each layer by starting at the layer $j+1$ with the water table and iterating upwards. θ_{j+1} can be determined by considering equilibrium soil moisture $\theta_{eq_{j+1}}$ (soil moisture corresponding to the scenario in which the water table is located exactly at the bottom of the soil layer, previously calculated in the model) and $\theta_{sat_{j+1}}$:

$$\theta_{j+1} = \theta_{sat_{j+1}} \frac{WTD - z_{j+1}}{\Delta z_{j+1}} + \theta_{eq_{j+1}} \frac{z_j - WTD}{\Delta z_{j+1}}. \tag{A2}$$

where z_j and z_{j+1} are the depths of soil layers j and $j+1$. From there, θ_j can be estimated by solving Eq. (A1) iteratively using the Newton–Raphson method, a numerical method that solves for the root of a well-behaved function (Press et al., 1992). In the next iteration, θ_j replaces θ_{j+1} and the new θ_j corresponds to the next layer (moving upwards). This continues until initial soil moisture values for remaining layers (until layer 4) are calculated.

Initial soil temperature values were obtained by linear interpolation. Initial values for the first 4 layers were provided by the WRF WPS input file, as well as a deep soil temperature initialization value corresponding to 8 m depth. We took this value as representative of 20 m depth (the bottom of the soil column in our modified Noah-MP simulations; F. Chen, personal communication, August 16, 2021), and estimated initial values for soil temperature in the additional layers based on this value and the initial value at the fourth layer (2 m depth).

Author contributions. C.A.B. prepared the manuscript with contributions from all co-authors. C.A.B. carried out the Noah-MP code modifications with contributions from G.M.M. The DynaRoot scheme was developed by Y.F. and G.M.M. C.A.B. completed simulations and analyses with contributions from F.D. F.D., Y.F. and G.M.M. were responsible for conceptualization of the study. F.D. supervised execution of the study and preparation of the manuscript.

Competing interests. The authors declare that they have no conflict of interest.

Acknowledgements. This material is based upon work supported by the National Science Foundation under Grant No. 1852707 and Grant No. 1852709. Any opinions, findings, and conclusions or recommendations expressed in this material are those of the author(s) and do not necessarily reflect the views of the National Science Foundation. C.A.B. gratefully acknowledges financial support for this research by the Fulbright U.S. Student Program, which is sponsored by the U.S. Department of State and the U.S.-Spain Fulbright Commission. The contents of this publication are solely the responsibility of the author and do not necessarily represent the official views of the Fulbright Program, the Government of the United States, or the U.S.-Spain Fulbright Commission. C.A.B. gratefully acknowledges financial support from the Alfred P. Sloan Foundation's Minority PhD Program. The HRLDAS modeling system was developed at the National Center for Atmospheric Research (NCAR). NCAR is sponsored by the United States National Science Foundation.

References

Amenu, G. G., Kumar, P., and Liang, X.-Z.: Interannual variability of deep-layer hydrologic memory and mechanisms of its influence on surface energy fluxes, Journal of Climate, 18, 5024–5045, https://doi.org/10.1175/JCLI3590.1, 2005.

Baker, I. T., Prihodko, L., Denning, A. S., Goulden, M., Miller, S., and Rocha, H. R. D.: Seasonal drought stress in the amazon: Reconciling models and observations, Journal of Geophysical Research: Biogeosciences, 114, https://doi.org/https://doi.org/10.1029/2007JG000644, 2009.

Baker, J. C., Garcia-Carreras, L., Gloor, M., Marsham, J. H., Buermann, W., da Rocha, H. R., Nobre, A. D., de Araujo, A. C., and Spracklen, D. V.: Evapotranspiration in the Amazon: spatial patterns, seasonality, and recent trends in observations, reanalysis, and climate models, Hydrology and Earth System Sciences, 25, 2279–2300, https://doi.org/https://doi.org/10.5194/hess-25-2279-2021, 2021.

Ball, J. T., Woodrow, I. E., and Berry, J. A.: A model predicting stomatal conductance and its contribution to the control of photosynthesis under different environmental conditions, in: Progress in photosynthesis research: Volume 4 Proceedings of the VIIth International Congress on Photosynthesis, Providence, Rhode Island, USA, August 10–15, 1986, pp. 221–224, Springer, https://doi.org/https://doi.org/10.1007/978-94-017-0519-6_48, 1987.

Balsamo, G., Pappenberger, F., Dutra, E., Viterbo, P., and Van den Hurk, B.: A revised land hydrology in the ECMWF model: A step towards daily water flux prediction in a fully-closed water cycle, Hydrological Processes, 25, 1046–1054, https://doi.org/https://doi.org/10.1002/hyp.7808, 2011.

Bao, J., Stevens, B., Kluft, L., and Muller, C.: Intensification of daily tropical precipitation extremes from more organized convection, Science Advances, 10, eadj6801, https://doi.org/DOI: 10.1126/sciadv.adj6801, 2024.

Barlage, M., Tewari, M., Chen, F., Miguez-Macho, G., Yang, Z.-L., and Niu, G.-Y.: The effect of groundwater interaction in North American regional climate simulations with WRF/Noah-MP, Climatic Change, 129, 485–498, 2015.

Barlage, M., Chen, F., Rasmussen, R., Zhang, Z., and Miguez-Macho, G.: The importance of scale-dependent groundwater processes in land-atmosphere interactions over the central United States, Geophysical Research Letters, 48, e2020GL092 171, 2021.

Batelis, S.-C., Rahman, M., Kollet, S., Woods, R., and Rosolem, R.: Towards the representation of groundwater in the Joint UK Land Environment Simulator, Hydrological processes, 34, 2843–2863, 2020.

Beaudoing, H., Rodell, M., and NASA/GSFC/HSL: GLDAS Noah Land Surface Model L4 3 hourly 0.25 x 0.25 degree, Version 2.1, https://doi.org/10.5067/E7TYRXPJKWOQ, 2020.

Best, M. J., Pryor, M., Clark, D., Rooney, G. G., Essery, R., Ménard, C., Edwards, J., Hendry, M., Porson, A., Gedney, N., et al.: The Joint UK Land Environment Simulator (JULES), model description–Part 1: energy and water fluxes, Geoscientific Model Development, 4, 677–699, 2011.

Bisht, G., Riley, W. J., Hammond, G. E., and Lorenzetti, D. M.: Development and evaluation of a variably saturated flow model in the global E3SM Land Model (ELM) version 1.0, Geoscientific Model Development, 11, 4085–4102, 2018.

Broedel, E., Tomasella, J., Cândido, L. A., and von Randow, C.: Deep soil water dynamics in an undisturbed primary forest in central Amazonia: Differences between normal years and the 2005 drought, Hydrological Processes, 31, 1749–1759, 2017.

Bruno, R. D., Da Rocha, H. R., De Freitas, H. C., Goulden, M. L., and Miller, S. D.: Soil moisture dynamics in an eastern Amazonian tropical forest, Hydrological Processes: An International Journal, 20, 2477–2489, 2006.

Caldwell, P. M., Terai, C. R., Hillman, B., Keen, N. D., Bogenschutz, P., Lin, W., Beydoun, H., Taylor, M., Bertagna, L., Bradley, A., et al.: Convection-permitting simulations with the E3SM global atmosphere model, Journal of Advances in Modeling Earth Systems, 13, e2021MS002 544, 2021.

Canadell, J., Jackson, R. B., Ehleringer, J., Mooney, H. A., Sala, O. E., and Schulze, E.-D.: Maximum rooting depth of vegetation types at the global scale, Oecologia, 108, 583–595, 1996.

Chen, F., Manning, K. W., Lemone, M. A., Trier, S. B., Alfieri, J. G., Roberts, R., Tewari, M., Niyogi, D., Horst, T. W., Oncley, S. P., Basara, J. B., and Blanken, P. D.: Description and evaluation of the characteristics of the NCAR high-resolution land data assimilation system, Journal of Applied Meteorology and Climatology, 46, 694–713, 2007.

Chen, S., Stark, S. C., Nobre, A. D., Cuartas, L. A., de Jesus Amore, D., Restrepo-Coupe, N., Smith, M. N., Chitra-Tarak, R., Ko, H., Nelson, B. W., et al.: Amazon forest biogeography predicts resilience and vulnerability to drought, Nature, pp. 1–7, 2024.

Christoffersen, B. O., Restrepo-Coupe, N., Arain, M. A., Baker, I. T., Cestaro, B. P., Ciais, P., Fisher, J. B., Galbraith, D., Guan, X., Gulden, L., van den Hurk, B., Ichii, K., Imbuzeiro, H., Jain, A., Levine, N., Miguez-Macho, G., Poulter, B., Roberti, D. R., Sakaguchi, K., Sahoo, A., Schaefer, K., Shi, M., Verbeeck, H., Yang, Z. L., Araújo, A. C., Kruijt, B., Manzi, A. O., da Rocha, H. R., von Randow, C., Muza, M. N., Borak, J., Costa, M. H., de Gonçalves, L. G. G., Zeng, X., and Saleska, S. R.: Mechanisms of water supply and vegetation demand govern the seasonality and magnitude of evapotranspiration in Amazonia and Cerrado, Agricultural and Forest Meteorology, 191, 33–50, 2014.

Clapp, R. B. and Hornberger, G. M.: Empirical equations for some soil hydraulic properties, Water Resources Research, 14, 601–604, 1978.

Computational and Information Systems Laboratory: Derecho: HPE Cray EX System (University Community Computing), https://doi.org/https://doi.org/10.5065/qx9a-pg09, 2024.

Cusack, D. F., Christoffersen, B., Smith-Martin, C. M., Andersen, K. M., Cordeiro, A. L., Fleischer, K., Wright, S. J., Guerrero-Ramírez, N. R., Lugli, L. F., McCulloch, L. A., et al.: Toward a coordinated understanding of hydro-biogeochemical root functions in tropical forests for application in vegetation models, New Phytologist, 2024.

Davidson, E., Lefebvre, P. A., Brando, P. M., Ray, D. M., Trumbore, S. E., Solorzano, L. A., Ferreira, J. N., Da, M. M., Bustamante, C., and Nepstad, D. C.: Carbon Inputs and Water Uptake in Deep Soils of an Eastern Amazon Forest, 2011.

Dominguez, F., Eiras-Barca, J., Yang, Z., Bock, D., Nieto, R., and Gimeno, L.: Amazonian Moisture Recycling Revisited Using WRF With Water Vapor Tracers, Journal of Geophysical Research: Atmospheres, 127, 2022.

Dominguez, F., Rasmussen, R., Liu, C., Ikeda, K., Prein, A., Varble, A., Arias, P. A., Bacmeister, J., Bettolli, M. L., Callaghan, P., et al.: Advancing South American Water and Climate Science through Multidecadal Convection-Permitting Modeling, Bulletin of the American Meteorological Society, 105, E32–E44, 2024.

Drewniak, B.: Simulating dynamic roots in the energy exascale earth system land model, Journal of Advances in Modeling Earth Systems, 11, 338–359, 2019.

ECMWF: IFS Documentation CY48R1 - Part IV: Physical Processes, 4, ECMWF, https://doi.org/10.21957/02054f0fbf, 2023.

Eyring, V., Bony, S., Meehl, G. A., Senior, C. A., Stevens, B., Stouffer, R. J., and Taylor, K. E.: Overview of the Coupled Model Intercomparison Project Phase 6 (CMIP6) experimental design and organization, Geoscientific Model Development, 9, 1937–1958, 2016.

Fan, Y., Miguez-Macho, G., Weaver, C. P., Walko, R., and Robock, A.: Incorporating water table dynamics in climate modeling: 1. Water table observations and equilibrium water table simulations, Journal of Geophysical Research: Atmospheres, 112, 2007.

Fan, Y., Li, H., and Miguez-Macho, G.: Global patterns of groundwater table depth, Science, 339, 940–943, 2013.

Fan, Y., Miguez-Macho, G., Jobbágy, E. G., Jackson, R. B., and Otero-Casal, C.: Hydrologic regulation of plant rooting depth, Proceedings of the National Academy of Sciences of the United States of America, 114, 10 572–10 577, 2017.

FAO/UNESCO: The FAO-UNESCO Soil Map of the World, https://www.fao.org/soils-portal/data-hub/soil-maps-and-databases/faounesco-soil-map-of-the-world/en/, 1971.

Feddes, R. A., Hoff, H., Bruen, M., Dawson, T., De Rosnay, P., Dirmeyer, P., Jackson, R. B., Kabat, P., Kleidon, A., Lilly, A., et al.: Modeling root water uptake in hydrological and climate models, Bulletin of the American Meteorological Society, 82, 2797–2810, 2001.

Feng, Z., Leung, L. R., Hardin, J., Terai, C. R., Song, F., and Caldwell, P.: Mesoscale convective systems in DYAMOND global convection-permitting simulations, Geophysical Research Letters, 50, e2022GL102 603, 2023.

Fersch, B., Senatore, A., Adler, B., Arnault, J., Mauder, M., Schneider, K., Völksch, I., and Kunstmann, H.: High-resolution fully coupled atmospheric–hydrological modeling: a cross-compartment regional water and energy cycle evaluation, Hydrology and Earth System Sciences, 24, 2457–2481, 2020.

Gash, J. and Nobre, C.: Climatic effects of Amazonian deforestation: Some results from ABRACOS, Bulletin of the American meteorological society, 78, 823–830, 1997.

Gayler, S., Wöhling, T., Grzeschik, M., Ingwersen, J., Wizemann, H.-D., Warrach-Sagi, K., Högy, P., Attinger, S., Streck, T., and Wulfmeyer, V.: Incorporating dynamic root growth enhances the performance of Noah-MP at two contrasting winter wheat field sites, Water Resources Research, 50, 1337–1356, 2014.

Gilbert, R. O.: Statistical methods for environmental pollution monitoring, John Wiley & Sons, 1987.

Golaz, J.-C., Van Roekel, L. P., Zheng, X., Roberts, A. F., Wolfe, J. D., Lin, W., Bradley, A. M., Tang, Q., Maltrud, M. E., Forsyth, R. M., et al.: The DOE E3SM Model Version 2: Overview of the physical model and initial model evaluation, Journal of Advances in Modeling Earth Systems, 14, e2022MS003 156, 2022.

He, C., Valayamkunnath, P., Barlage, M., Chen, F., Gochis, D., Cabell, R., Schneider, T., Rasmussen, R., Niu, G.-Y., Yang, Z.-L., et al.: Modernizing the open-source community Noah with multi-parameterization options (Noah-MP) land surface model (version 5.0) with enhanced modularity, interoperability, and applicability, Geoscientific Model Development, 16, 5131–5151, 2023.

Honey, M.: Mapping Tree and Shrub Cover on Pastures in Rondônia, Brazil, M.s. thesis, San Diego State University, https://www.proquest.com/dissertations-theses/mapping-tree-shrub-cover-on-pastures-rondÃt'nia/docview/2819930021/se-2, 2023.

Huffman, G., Stocker, E., Bolvin, D., Nelkin, E., and Tan, J.: GPM IMERG Final Precipitation L3 Half Hourly 0.1 degree x 0.1 degree V07, Greenbelt, MD, https://doi.org/10.5067/GPM/IMERG/3B-HH/07, accessed: 02/01/2024, 2023.

Ivanov, V. Y., Hutyra, L. R., Wofsy, S. C., Munger, J. W., Saleska, S. R., Oliveira, R. C. D., and Camargo, P. B. D.: Root niche separation can explain avoidance of seasonal drought stress and vulnerability of overstory trees to extended drought in a mature Amazonian forest, Water Resources Research, 48, 2012.

Jain, A., Yang, X., Kheshgi, H., McGuire, A. D., Post, W., and Kicklighter, D.: Nitrogen attenuation of terrestrial carbon cycle response to global environmental factors, Global Biogeochemical Cycles, 23, 2009.

Jipp, P. H., Nepstad, D. C., Cassel, D., and Reis de Carvalho, C.: Deep soil moisture storage and transpiration in forests and pastures of seasonally-dry Amazonia, Climatic Change, 39, 395–412, 1998.

Joetzjer, E., Douville, H., Delire, C., and Ciais, P.: Present-day and future Amazonian precipitation in global climate models: CMIP5 versus CMIP3, Climate Dynamics, 41, 2921–2936, 2013.

Joetzjer, E., Maignan, F., Chave, J., Goll, D., Poulter, B., Barichivich, J., Maréchaux, I., Luyssaert, S., Guimberteau, M., Naudts, K., et al.: Effect of tree demography and flexible root water uptake for modeling the carbon and water cycles of Amazonia, Ecological modelling, 469, 109 969, 2022.

Jucker, M., Lane, T., Vincent, C., Webster, S., Wales, S., and Louf, V.: Locally forced convection in subkilometre-scale simulations with the Unified Model and WRF, Quarterly Journal of the Royal Meteorological Society, 146, 3450–3465, 2020.

Kendall, M. G.: Rank correlation methods., 1948.

Kendon, E., Prein, A., Senior, C., and Stirling, A.: Challenges and outlook for convection-permitting climate modelling, Philosophical Transactions of the Royal Society A, 379, 20190 547, 2021.

Kennedy, D., Swenson, S., Oleson, K. W., Lawrence, D. M., Fisher, R., Lola da Costa, A. C., and Gentine, P.: Implementing plant hydraulics in the community land model, version 5, Journal of Advances in Modeling Earth Systems, 11, 485–513, 2019.

Kim, Y., Knox, R. G., Longo, M., Medvigy, D., Hutyra, L. R., Pyle, E. H., Wofsy, S. C., Bras, R. L., and Moorcroft, P. R.: Seasonal carbon dynamics and water fluxes in an Amazon rainforest, Global Change Biology, 18, 1322–1334, 2012.

Kleidon, A. and Heimann, M.: Assessing the role of deep rooted vegetation in the climate system with model simulations: mechanism, comparison to observations and implications for Amazonian deforestation, 2000.

Krinner, G., Viovy, N., de Noblet-Ducoudré, N., Ogée, J., Polcher, J., Friedlingstein, P., Ciais, P., Sitch, S., and Prentice, I. C.: A dynamic global vegetation model for studies of the coupled atmosphere-biosphere system, Global Biogeochemical Cycles, 19, 2005.

Lawrence, D. M., Fisher, R. A., Koven, C. D., Oleson, K. W., Swenson, S. C., Bonan, G., Collier, N., Ghimire, B., van Kampenhout, L., Kennedy, D., et al.: The Community Land Model version 5: Description of new features, benchmarking, and impact of forcing uncertainty, Journal of Advances in Modeling Earth Systems, 11, 4245–4287, 2019.

Li, L., Yang, Z.-L., Matheny, A. M., Zheng, H., Swenson, S. C., Lawrence, D. M., Barlage, M., Yan, B., McDowell, N. G., and Leung, L. R.: Representation of plant hydraulics in the Noah-MP land surface model: Model development and multiscale evaluation, Journal of Advances in Modeling Earth Systems, 13, e2020MS002 214, 2021.

Lin, T.-S.: Modeling the effects of environmental and management variables on crop productivity, Ph.D. thesis, University of Illinois at Urbana-Champaign, 2022.

Lin, T.-S., Kheshgi, H. S., Song, Y., Vörösmarty, C. J., and Jain, A. K.: Which crop has the highest bioethanol yield in the United States?, Frontiers in Energy Research, 11, 2023.

Liu, T., Chen, D., Yang, L., Meng, J., Wang, Z., Ludescher, J., Fan, J., Yang, S., Chen, D., Kurths, J., et al.: Teleconnections among tipping elements in the Earth system, Nature Climate Change, 13, 67–74, 2023.

Liu, X., Chen, F., Barlage, M., and Niyogi, D.: Implementing dynamic rooting depth for improved simulation of soil moisture and land surface feedbacks in Noah-MP-Crop, Journal of Advances in Modeling Earth Systems, 12, e2019MS001 786, 2020.

Mann, H. B.: Nonparametric tests against trend, Econometrica: Journal of the econometric society, pp. 245–259, 1945.

Markewitz, D., Devine, S., Davidson, E. A., Brando, P., and Nepstad, D. C.: Soil moisture depletion under simulated drought in the Amazon: Impacts on deep root uptake, New Phytologist, 187, 592–607, 2010.

Martens, B., Miralles, D. G., Lievens, H., Van Der Schalie, R., De Jeu, R. A., Fernández-Prieto, D., Beck, H. E., Dorigo, W. A., and Verhoest, N. E.: GLEAM v3: Satellite-based land evaporation and root-zone soil moisture, Geoscientific Model Development, 10, 1903–1925, 2017.

Martinez, J. A., Dominguez, F., and Miguez-Macho, G.: Effects of a groundwater scheme on the simulation of soil moisture and evapotranspiration over southern South America, Journal of Hydrometeorology, 17, 2941–2957, 2016a.

Martinez, J. A., Dominguez, F., and Miguez-Macho, G.: Impacts of a groundwater scheme on hydroclimatological conditions over southern South America, Journal of Hydrometeorology, 17, 2959–2978, 2016b.

Miguez-Macho, G. and Fan, Y.: The role of groundwater in the Amazon water cycle: 1. Influence on seasonal streamflow, flooding and wetlands, Journal of Geophysical Research Atmospheres, 117, 2012.

Miguez-Macho, G. and Fan, Y.: Spatiotemporal origin of soil water taken up by vegetation, Nature, 598, 624–628, 2021.

Miguez-Macho, G., Fan, Y., Weaver, C. P., Walko, R., and Robock, A.: Incorporating water table dynamics in climate modeling: 2. Formulation, validation, and soil moisture simulation, Journal of Geophysical Research Atmospheres, 112, 2007.

Milly, P. C., Malyshev, S. L., Shevliakova, E., Dunne, K. A., Findell, K. L., Gleeson, T., Liang, Z., Phillipps, P., Stouffer, R. J., and Swenson, S.: An enhanced model of land water and energy for global hydrologic and earth-system studies, Journal of Hydrometeorology, 15, 1739–1761, 2014.

Miralles, D. G., Holmes, T., De Jeu, R., Gash, J., Meesters, A., and Dolman, A.: Global land-surface evaporation estimated from satellite-based observations, Hydrology and Earth System Sciences, 15, 453–469, 2011.

Morton, D. C., Nagol, J., Carabajal, C. C., Rosette, J., Palace, M., Cook, B. D., Vermote, E. F., Harding, D. J., and North, P. R.: Amazon forests maintain consistent canopy structure and greenness during the dry season, Nature, 506, 221–224, 2014.

Naudts, K., Ryder, J., McGrath, M. J., Otto, J., Chen, Y., Valade, A., Bellasen, V., Berhongaray, G., Bönisch, G., Campioli, M., et al.: A vertically discretised canopy description for ORCHIDEE (SVN r2290) and the modifications to the energy, water and carbon fluxes, Geoscientific Model Development, 8, 2035–2065, 2015.

Nepstad, D. C.: The effects of partial throughfall exclusion on canopy processes, aboveground production, and biogeochemistry of an Amazon forest, Journal of Geophysical Research, 107, 2002.

Nepstad, D. C., de Carvalho, C. R., Davidson, E. A., Jipp, P. H., Lefebvre, P. A., Negreiros, G. H., da Silva, E. D., Stone, T. A., Trumbore, S. E., and Vieira, S.: The role of deep roots in the hydrological and carbon cycles of Amazonian forests and pastures, Nature, 372, 666–669, 1994.

Nepstad, D. C., Tohver, I. M., David, R., Moutinho, P., and Cardinot, G.: Mortality of large trees and lianas following experimental drought in an amazon forest, Ecology, 88, 2259–2269, 2007.

Niu, G. Y., Yang, Z. L., Mitchell, K. E., Chen, F., Ek, M. B., Barlage, M., Kumar, A., Manning, K., Niyogi, D., Rosero, E., Tewari, M., and Xia, Y.: The community Noah land surface model with multiparameterization options (Noah-MP): 1. Model description and evaluation with local-scale measurements, Journal of Geophysical Research Atmospheres, 116, 2011.

Niu, G.-Y., Fang, Y.-H., Chang, L.-L., Jin, J., Yuan, H., and Zeng, X.: Enhancing the Noah-MP ecosystem response to droughts with an explicit representation of plant water storage supplied by dynamic root water uptake, Journal of Advances in Modeling Earth Systems, 12, e2020MS002 062, 2020.

Oleson, K., Lawrence, D., Bonan, G., Drewniack, B., Huang, M., Koven, C., Levis, S., Li, F., Riley, W., Subin, Z., et al.: Technical description of version 4.5 of the Community Land Model (CLM)(Technical Note No. NCAR/TN-503+ STR). Boulder, CO: National Center for Atmospheric Research Earth System Laboratory, 2013.

Oliveira, R., Bezerra, L., Davidson, E., Pinto, F., Klink, C., Nepstad, D., and Moreira, A.: Deep root function in soil water dynamics in cerrado savannas of central Brazil, Functional Ecology, 19, 574–581, 2005a.

Oliveira, R. S., Dawson, T. E., Burgess, S. S., and Nepstad, D. C.: Hydraulic redistribution in three Amazonian trees, Oecologia, 145, 354–363, 2005b.

Peng, S., De Weirdt, M., and Verbeeck, H.: Two soil hydrology formulations of ORCHIDEE (version Trunk. rev1311) tested for the Amazon basin, 2014.

Piontekowski, V. J., Ribeiro, F. P., Matricardi, E. A. T., Lustosa Junior, I. M., Bussinguer, A. P., and Gatto, A.: Modeling deforestation in the state of Rondônia, Floresta e Ambiente, 26, e20180 441, 2019.

Pitman, A.: The evolution of, and revolution in, land surface schemes designed for climate models, International Journal of Climatology: A Journal of the Royal Meteorological Society, 23, 479–510, 2003.

Press, W. H., Teukolsky, S. A., Vetterling, W. T., and Flannery, B. P.: Numerical recipes in FORTRAN : the art of scientific computing, Cambridge University Press, 1992.

Qiu, H., Bisht, G., Li, L., Hao, D., and Xu, D.: Development of inter-grid cell lateral unsaturated and saturated flow model in the E3SM land model (v2. 0), EGUsphere, 2023, 1–31, 2023.

Rehbein, A., Ambrizzi, T., and Mechoso, C. R.: Mesoscale convective systems over the Amazon basin. Part I: climatological aspects, International Journal of Climatology, 38, 215–229, 2018.

Reick, C. H., Gayler, V., Goll, D., Hagemann, S., Heidkamp, M., Nabel, J. E., Raddatz, T., Roeckner, E., Schnur, R., and Wilkenskjeld, S.: JSBACH 3-The land component of the MPI Earth System Model: documentation of version 3.2, 2021.

Restom, T. G. and Nepstad, D. C.: Seedling growth dynamics of a deeply rooting liana in a secondary forest in eastern Amazonia, 190, 109–118, 2004.

Restrepo-Coupe, N., da Rocha, H., Hutyra, L., de Araujo, A., Borma, L., Christoffersen, B., Cabral, O., de Camargo, P., Cardoso, F., Costa, A., Fitzjarrald, D., Goulden, M., Kruijt, B., Maia, J., Malhi, Y., Manzi, A., Miller, S., Nobre, A., von Randow, C., Abreu Safaj, L., Sakai, R., Tota, J., Wofsy, S., Zanchi, F., and Saleska, S.: LBA-ECO CD-32 Flux Tower Network Data Compilation, Brazilian Amazon: 1999-2006, V2, https://doi.org/10.3334/ORNLDAAC/1842, 2021.

Roberts, D., Numata, I., Holmes, K., Batista, G., Krug, T., Monteiro, A., Powell, B., and Chadwick, O.: Large area mapping of land-cover change in Rondônia using multitemporal spectral mixture analysis and decision tree classifiers, Journal of Geophysical Research: Atmospheres, 107, LBA–40, 2002.

Rodell, B. M., Houser, P. R., Jambor, U., Gottschalck, J., Mitchell, K., j Meng, C., Arsenault, K., Cosgrove, B., Radakovich, J., Bosilovich, M., Entin, J. K., Walker, J. P., Lohmann, D., and Toll, D.: THE GLOBAL LAND DATA ASSIMILATION SYSTEM This powerful new land surface modeling system integrates data from advanced observing systems to support improved forecast model initialization and hydrometeorological investigations, 2004.

Sakaguchi, K. and Zeng, X.: Effects of soil wetness, plant litter, and under-canopy atmospheric stability on ground evaporation in the Community Land Model (CLM3. 5), Journal of Geophysical Research: Atmospheres, 114, 2009.

Sakschewski, B., Von Bloh, W., Boit, A., Poorter, L., Peña-Claros, M., Heinke, J., Joshi, J., and Thonicke, K.: Resilience of Amazon forests emerges from plant trait diversity, Nature Climate Change, 6, 1032–1036, https://doi.org/10.1038/nclimate3109, 2016.

Saleska, S. R., Didan, K., Huete, A. R., and Rocha, H. R. D.: Amazon forests green-up during 2005 drought, Science, 318, 612, 2007.

Satoh, M., Stevens, B., Judt, F., Khairoutdinov, M., Lin, S.-J., Putman, W. M., and Düben, P.: Global cloud-resolving models, Current Climate Change Reports, 5, 172–184, 2019.

Schneck, R., Gayler, V., Nabel, J. E., Raddatz, T., Reick, C. H., and Schnur, R.: Assessment of JSBACHv4. 30 as a land component of ICON-ESM-V1 in comparison to its predecessor JSBACHv3. 2 of MPI-ESM1. 2, Geoscientific Model Development, 15, 8581–8611, 2022.

Schwitalla, T., Warrach-Sagi, K., Wulfmeyer, V., and Resch, M.: Near-global-scale high-resolution seasonal simulations with WRF-Noah-MP v. 3.8. 1, Geoscientific Model Development, 13, 1959–1974, 2020.

Sen, P. K.: Estimates of the regression coefficient based on Kendall's tau, Journal of the American statistical association, 63, 1379–1389, 1968.

Shahi, N. K., Polcher, J., Bastin, S., Pennel, R., and Fita, L.: Assessment of the spatio-temporal variability of the added value on precipitation of convection-permitting simulation over the Iberian Peninsula using the RegIPSL regional earth system model, Climate Dynamics, 59, 471–498, 2022.

Shevliakova, E., Malyshev, S., Martinez-Cano, I., Milly, P., Pacala, S., Ginoux, P., Dunne, K., Dunne, J., Dupuis, C., Findell, K., et al.: The land component LM4. 1 of the GFDL Earth System Model ESM4. 1: Model description and characteristics of land surface climate and carbon cycling in the historical simulation, Journal of Advances in Modeling Earth Systems, 16, e2023MS003 922, 2024.

Singh, C., Wang-Erlandsson, L., Fetzer, I., Rockström, J., and Van Der Ent, R.: Rootzone storage capacity reveals drought coping strategies along rainforest-savanna transitions, Environmental Research Letters, 15, 124 021, 2020.

Skamarock, W. C., Klemp, J. B., Dudhia, J., Gill, D. O., Liu, Z., Berner, J., Wang, W., Powers, J. G., Duda, M. G., Barker, D. M., and Huang, X.-Y.: A Description of the Advanced Research WRF Model Version 4.3, https://doi.org/10.5065/1DFH-6P97, 2021.

Smith, T. and Boers, N.: Global vegetation resilience linked to water availability and variability, Nature Communications, 14, 2023.

Song, Y., Jain, A., and McIsaac, G.: Implementation of dynamic crop growth processes into a land surface model: evaluation of energy, water and carbon fluxes under corn and soybean rotation, Biogeosciences, 10, 8039–8066, 2013.

Song, Y., Cervarich, M., Jain, A. K., Kheshgi, H. S., Landuyt, W., and Cai, X.: The interplay between bioenergy grass production and water resources in the United States of America, Environmental Science & Technology, 50, 3010–3019, 2016.

Spera, S. A., Winter, J. M., and Chipman, J. W.: Evaluation of agricultural land cover representations on regional climate model simulations in the Brazilian Cerrado, Journal of Geophysical Research: Atmospheres, 123, 5163–5176, 2018.

Theil, H.: A rank-invariant method of linear and polynomial regression analysis, Indagationes mathematicae, 12, 173, 1950.

van Oorschot, F., van der Ent, R. J., Hrachowitz, M., and Alessandri, A.: Climate controlled root zone parameters show potential to improve water flux simulations by land surface models, Earth System Dynamics Discussions, 2021, 1–26, 2021.

Verbeeck, H., Peylin, P., Bacour, C., Bonal, D., Steppe, K., and Ciais, P.: Seasonal patterns of CO2 fluxes in Amazon forests: Fusion of eddy covariance data and the ORCHIDEE model, Journal of Geophysical Research: Biogeosciences, 116, 2011.

Von Randow, C., Manzi, A. O., Kruijt, B., De Oliveira, P., Zanchi, F. B., Silva, R. d., Hodnett, M. G., Gash, J. H., Elbers, J. A., Waterloo, M., et al.: Comparative measurements and seasonal variations in energy and carbon exchange over forest and pasture in South West Amazonia, Theoretical and Applied Climatology, 78, 5–26, 2004.

von Randow, C., Manzi, A. O., Kruijt, B., de Oliveira, P. J., Zanchi, F. B., Silva, R. L., Hodnett, M. G., Gash, J. H., Elbers, J. A., Waterloo, M. J., Cardoso, F. L., and Kabat, P.: Comparative measurements and seasonal variations in energy and carbon exchange over forest and pasture in South West Amazonia, Theoretical and Applied Climatology, 78, 5–26, 2004.

Wang, P., Niu, G.-Y., Fang, Y.-H., Wu, R.-J., Yu, J.-J., Yuan, G.-F., Pozdniakov, S. P., and Scott, R. L.: Implementing dynamic root optimization in Noah-MP for simulating phreatophytic root water uptake, Water Resources Research, 54, 1560–1575, 2018.

Wei, Z., Yoshimura, K., Wang, L., Miralles, D. G., Jasechko, S., and Lee, X.: Revisiting the contribution of transpiration to global terrestrial evapotranspiration, Geophysical Research Letters, 44, 2792–2801, 2017.

Werth, D. and Avissar, R.: The local and global effects of Amazon deforestation, Journal of Geophysical Research: Atmospheres, 107, LBA–55, 2002.

Wiltshire, A. J., Duran Rojas, M. C., Edwards, J. M., Gedney, N., Harper, A. B., Hartley, A. J., Hendry, M. A., Robertson, E., and Smout-Day, K.: JULES-GL7: the Global Land configuration of the Joint UK Land Environment Simulator version 7.0 and 7.2, Geoscientific Model Development, 13, 483–505, 2020.

Yao, Y., Joetzjer, E., Ciais, P., Viovy, N., Cresto Aleina, F., Chave, J., Sack, L., Bartlett, M., Meir, P., Fisher, R., et al.: Forest fluxes and mortality response to drought: model description (ORCHIDEE-CAN-NHA, r7236) and evaluation at the Caxiuanã drought experiment, Geoscientific Model Development Discussions, 2021, 1–38, 2022.

Zanin, P. R.: Soil Water Uptake by Amazonian Trees and Simulation of Impacts on Energy Fluxes and Soil Moisture Dynamics at the LBA Flux Towers, Revista Brasileira de Meteorologia, 36, 441–454, 2021.

Zemp, D. C., Schleussner, C. F., Barbosa, H. M., Ent, R. J. V. D., Donges, J. F., Heinke, J., Sampaio, G., and Rammig, A.: On the importance of cascading moisture recycling in South America, Atmospheric Chemistry and Physics, 14, 13 337–13 359, 2014.

Zilli, M. T., Lemes, M. R., Hart, N. C. G., et al.: The added value of using convective-permitting regional climate model simulations to represent cloud band events over South America, Climate Dynamics, 62, 10 543–10 564, https://doi.org/10.1007/s00382-024-07460-3, 2024.

Table 1. Summary of representation of deep, dynamic RWU, groundwater (GW) dynamics, and capability of CPM coupling in existing land surface models. We consider deep RWU to be RWU that occurs at 5 m or below. We consider dynamic RWU to be RWU that changes with time and/or moisture content.

Model	Number of soil layers	Cumulative depth of soil layers	Deep RWU?	Dynamic RWU?	GW scheme?	Couple with CPM?	Relevant publications
Noah-Multiparameterization Model (Noah-MP)	4	2 m	No	No	Yes	Yes	Niu et al. (2011); He et al. (2023)
Integrated Science Assessment Model (ISAM)	15	50 m (total); 3.5 m hydrologically active	No	Yes	No	Yes	Jain et al. (2009); Song et al. (2013); Song et al. (2016); Lin (2022); Lin et al. (2023)
Community Land Model (CLM)	25	About 50 m (total); 8.5 m hydrologically active	Yes	Yes	Yes	Yes	Lawrence et al. (2019); Kennedy et al. (2019)
Energy Exascale Earth System Model (E3SM) Land Model (ELM)	15	42.1 m (total); 3.8 m hydrologically active	No	Yes	Yes	Yes	Oleson et al. (2013); Bisht et al. (2018); Drewniak (2019); Caldwell et al. (2021); Golaz et al. (2022); Qiu et al. (2023)
Jena Scheme for Biosphere-Atmosphere Coupling in Hamburg (JSBACH)	5	9.8 m	Yes	No	No	Yes	Reick et al. (2021); Schneck et al. (2022); Bao et al. (2024)
Revised Hydrology for the Tiled ECMWF Scheme for Surface Exchanges over Land (HTESSEL)	4	2.89 m	No	No	No	No	Balsamo et al. (2011); ECMWF (2023)
Organizing Carbon and Hydrology in Dynamic Ecosystems (ORCHIDEE)	12	4 m	Yes	Yes	No	Yes	Krinner et al. (2005); Verbeeck et al. (2011); Peng et al. (2014); Naudts et al. (2015); Yao et al. (2022); Shahi et al. (2022); Joetzjer et al. (2022)
Joint UK Land Environment Simulator (JULES)	4	3 m	No	No	No	Yes	Best et al. (2011); Batelis et al. (2020); Jucker et al. (2020); Wiltshire et al. (2020)
Geophysical Fluid Dynamics Laboratory (GFDL) Land Model (LM)	Variable; 20 in Milly et al. (2014)	Variable; 10 m in Shevliakova et al. (2024)	Yes	Yes	Yes	No	Milly et al. (2014); Shevliakova et al. (2024) Cusack et al. (2024)

Table 2. Summary of existing representations of deep, dynamic RWU in land surface models and how they compare with our approach.

Reference	Model used	Deep RWU?	Dynamic RWU?	Difference from our study
Gayler et al. (2014)	Noah-MP	No	Yes	Does not include representation of deep RWU
Niu et al. (2020)	Noah-MP	No	Yes	Does not include representation of deep RWU
Liu et al. (2020)	Noah-MP	No	Yes	Does not include representation of deep RWU; implemented in the Noah-MP-Crop model and less applicable to study of forest ecosystems
Wang et al. (2018)	Noah-MP	Yes	Yes	We seek to implement a lower-complexity scheme that can be easily scaled up to a continental domain
Li et al. (2021)	Noah-MP	Yes	Yes	
Zanin (2021)	Noah (coupled with Eta/CPTEC regional climate model)	Yes	No	Does not include representation of dynamic RWU; we place more emphasis on the role of drainage gradient
van Oorschot et al. (2021)	HTESSEL	No	Yes	Does not include representation of deep RWU; we focus on enhancing RWU directly

Table 3. Soil layer depths as defined in modified Noah-MP simulations (our SOIL and ROOT experiments). Layers in bold are identical to the layers in unmodified (default) Noah-MP (our FD and GW experiments).

Layer number	Depth of layer bottom (m)
1	**0.1**
2	**0.4**
3	**1**
4	**2**
5	3
6	4
7	6
8	8
9	10
10	12
11	15
12	20

Table 4. Noah-MP cases analyzed in this study.

Simulation name	Description
FD (Control)	Unmodified Noah-MP run with free drainage groundwater option (RUNOFF_OPTION=3)
GW	Unmodified Noah-MP run with the Miguez-Macho and Fan (MMF) groundwater scheme (RUNOFF_OPTION=5; Miguez-Macho et al. 2007)
SOIL	Modified Noah-MP with additional soil layers and soil properties varying with depth
ROOT	Identical to SOIL but with DynaRoot activated

Table 5. Technical specifications and selected Noah-MP settings for all simulations. A copy of the namelist file used in our simulations is provided with our modified Noah-MP code (see code availability section below).

Simulation length	Jun 2000 to Dec 2019 (about 20 years)
Horizontal resolution	4 km
Forcing time step	3 h
Model time step	30 min
Atmospheric forcing data (Temperature, wind speed, incoming shortwave radiation, incoming longwave radiation, surface pressure, and specific humidity)	GLDAS V2.1 Level 4 Noah Land Surface Model 3 hourly $0.25^\circ \times 0.25^\circ$ product (Beaudoing et al., 2020)
Atmospheric forcing data (Precipitation)	GPM IMERG Final Precipitation L3 Half Hourly $0.1^\circ \times 0.1^\circ$ V07 product (Huffman et al., 2023)
Initialization file	WRF WPS input file
DYNAMIC_VEG_OPTION	Dynamic vegetation model inactive; use vegetation fraction from input data and monthly-mean LAI (Option 7)
CANOPY_STOMATAL_RESISTANCE_OPTION	Ball-Berry (Ball et al., 1987) (Option 1)
BTR_OPTION	Noah-type (Niu et al., 2011) (Option 1)
SURFACE_DRAG_OPTION	Monin-Obukhov (Option 1)
TBOT_OPTION	Temperature at soil bottom (TBOT) read from file (Option 2)
SURFACE_RESISTANCE_OPTION	Sakaguchi and Zeng (2009) (Option 1)